Desalination and Water Treatment
www.deswater.com
doi: 10.5004/dwt.2021.27507

232 (2021) 165–186
August

Understanding the electrokinetic behavior of the acrylic acid-based Fe(II) ion-imprinted polymer for its application in Fe(II) ions removal from aqueous medium with high selectivity

Tanveer ul Haq Zia[a,*], Daud Khan Ghazali[a], Behisht Ara[b], Kashif Gul[b], Muhammad Hassaan Qureshi[a], Nauman Ali[b]

[a]*Department of Chemistry, Sarhad University of Science and IT, Landi Akhun Ahmad, Hayatabad Link Ring Road, Peshawar (Khyber Pakhtunkhwa), 25000 Pakistan, Tel. +92-334 9011757; emails: tanveerics@gmail.com (T. ul Haq Zia), daudtoofaan@gmail.com (D.K. Ghazali), mhq2310@gmail.com (M.H. Qureshi)*
[b]*Institute of Chemical Sciences, University of Peshawar, Jamrud Road, Peshawar (Khyber Pakhtunkhwa), 25120 Pakistan, emails: bahishtara@gmail.com (B. Ara), kashifpkh@yahoo.com (K. Gul), nali75pk@upesh.edu.pk (N. Ali)*

Received 12 November 2020; Accepted 4 June 2021

ABSTRACT

Electrokinetic analysis was carried out to study the nature of the electrostatic potential ζ at the adsorbent surface as a function of surface charge density σ to understand the interaction between adsorbate and adsorbent. In the present study, precipitation polymerization was carried out in acetonitrile for preparing an ion-imprinted polymer [Fe(II) IIP] for Fe(II) ions by using acrylic acid as functional monomer, the crosslinking agent was N,N′-Methylenebis(acrylamide), 1,10-phenanthroline as chelating agent for Fe(II) ions and azobisisobutyronitrile as thermal initiator. The ion-imprinted polymer [Fe(II) IIP] which was obtained after performing the leaching for Fe(II) ions removal, displayed a greater affinity for selective recombination with the Fe(II) ions as a target analyte. The morphological analysis was performed by applying scanning electron microscopy while the Fourier-transform infrared spectroscopy was employed to illustrate the different functional groups which are present in the structure of the molecule. Similarly, the specific surface area was determined to be 473.44 $m^2\ g^{-1}$ for non-imprinted polymer (NIP) whereas 585.04 $m^2\ g^{-1}$ for Fe(II) IIP by employing the Brunauer–Emmett–Teller (BET) model. Furthermore, the Barrett, Joyner, Halenda model and *t*-plot method was used for evaluating the pore size distribution that illustrated the surface texture nature to be mesoporous for both adsorbents. Langmuir, Freundlich, Dubinin–Radushkevich and BET adsorption models were applied to the equilibrium adsorption data for understanding the adsorption process. It was found that the adsorbent has a heterogeneous surface as the Freundlich isotherm model was obeyed more closely by both the adsorbents. The maximum adsorption capacity of 4.176 mg g^{-1} was reported for NIP in comparison to 5.559 mg g^{-1} in the case of the Fe(II) IIP. For the metal ion pairs of Fe(II)/Co(II), Fe(II)/Cu(II), Fe(II)/Ni(II) and Fe(II)/Pb(II), the relative selectivity coefficient *k*′ was found to be 32.412, 1.129, 1.508 and 1.264, respectively. The adsorption kinetic data followed the pseudo-second-order kinetics more closely pointing to the multistep mechanism of adsorption depicting the substrate and analyte dependency. Also, the Van't Hoff plot was applied in order to determine the change in entropy (ΔS), enthalpy (ΔH) and Gibbs free energy (ΔG) as thermodynamic parameters.

Keywords: Fe(II) ions; Ion imprinting; Electrokinetic; Barrett, Joyner, Halenda and Brunauer–Emmett–Teller; Langmuir; Thermal initiator; Precipitation polymerization; Relative selectivity coefficient

* Corresponding author.

1. Introduction

The use of heavy metals has been increased in recent years which is the cause of many health issues around the globe [1]. Various heavy metals are also required in trace amounts for many biological functions as they play a vital role in the redox and enzymatic reactions occurring in living organisms. But the excess amount of these metals may cause serious damages in tissues and cells which make the possibility of certain disorders in human beings [2]. Many of its harmful effects on the cellular level have been reported as they are responsible for the damage of cellular organelles and the nucleus of the cell. They also disturb the function of enzymes which may lead to disorders in metabolism, repair mechanism and detoxification [3].

These metals can be removed through various techniques from aqueous and non-aqueous solutions. For many years, suitable removal methods have always been needed which could overcome the limitations of cost, reusability, sludge formation and time consumption. One of the most reliable techniques is using imprinted polymer (IPs) which was first introduced in 1972, whose widespread applications were discovered later on [4]. The polymer is processed with a technique called Molecular Imprinting Technique to make the template-shaped cavities in the polymer, which make it highly selective to the target analyte [5]. The IPs provide the binding sites to the target analyte with functional groups having complementary shapes and sizes [6]. Due to its high recognition, the IPs have been successfully applied in a variety of fields such as controlled drug delivery, catalysis, affinity separation, metal ions removal and chemical sensing [7–9]. The IPs provide more fast and reliable results as compared to classical liquid-liquid phase and solid-phase extraction procedures [10]. They have the ability to mimic natural perceptions like biological receptors and antibodies [11]. Molecular imprinted solid-phase extraction is a low-cost and high stability technique giving better selectivity and applicability to the analyte to form complex even at trace level. The molecular imprinting technique coupled with the solid phase extraction enhanced the efficacy to great extent [12]. Binding sites of these molecularly imprinted polymers (MIPs) provide distinct characteristics which depend upon the interactions created among the template and monomer in the course of polymerization [13]. The molecularly imprinted polymers (MIP) for the metal ions will be interpreted as ion-imprinted polymers (IIP) [14].

The template has the central importance in the process of molecular imprinting which guides the association of functional monomers and cross-linker in a pattern of desired shape and size. Traditionally templates are small molecules or ions which are chemically inert during polymerization. It determines the level of selectivity and recognition of molecularly imprinted polymer [15]. The selection of monomers depends upon the nature of the template and the type of polymerization reaction. The interaction between the monomer and template is due to the functional groups of the monomer [16].

The cross-linker is used to lock the functional groups of the monomers on the desired positions and tracks across the template in order to preserve the cavities and provide rigidity and strength to the imprinted polymer (IPs). The role of the cross-linker is not only to provide structural stability but also to stabilize the binding sites mechanically. The nature of cross-linker determines the physical and chemical properties and degree of cross-linking of the IPs [17].

The ion-imprinted polymers are prepared through various techniques such as bulk polymerization, precipitation polymerization, suspension polymerization and surface imprinted technique [18,19]. Among them, the reliable method for preparing the imprinted polymers is precipitation polymerization. With this technique polymer of uniform shape and size can be synthesized by using a homogeneous mixture of initiator, monomers and solvents followed by precipitation of polymer from the mixture [20]. The size of polymer particles depends upon the solvent as in poor solvents its size is in micrometer while it produces turbid macroscopic gels in good solvents [21]. It is comparatively a simpler way of synthesizing imprinted polymers in a poor solvent at high dilution [22].

Iron is one of the essential elements required for almost all living organisms [23]. It is an important nutritional element playing a vital role in cellular respiration, electron transport chain and cell proliferation [24]. It is very useful and used in many fields like making magnets, abrasives, pigments, steel and polishing compounds. Iron is biologically very effective due to its chemical properties, that is, its valency, complex formation and solubility. Environmental pollution in the form of heavy metal ions has severe negative effects on living organisms. The organic and inorganic species present in the liquid and solid are separated and preconcentrated by applying a broad diversity of methods such as flocculation, filtration and precipitation which have severe shortcomings of sludge formation and fowling [25]. Therefore, the removal of heavy metal ions is an important obligation that requires state of art technology of solid-phase extraction for its recovery from aqueous as well as non-aqueous solutions. As ferric ion is stable in nature but forms compounds such as iron(III) oxide-hydroxide that are insoluble in water, at and around pH 7 [26]. A suitable adsorbent is required for analytical applications in aqueous solutions of higher pH with oxygen-poor conditions for evaluation of iron in ferrous form as ferric form precipitates out mostly at higher pH [27]. In addition, it is important to mention here that an analytical determination of ferrous ions in matrices of different nature is an important task that requires an adsorbent selectively tuned for it. Similarly, the presence of ferrous ions in certain compounds reduces their optical properties due to which it should be removed prior to manufacturing devices [28]. The polymers which are ion-imprinted will be used for solid-phase extraction of very low concentrations of target analytes which will render it an appropriate candidate for pre-concentration level. Previously, the surface imprinting technique has been applied to prepare a Fe(III) ion-imprinted silica gel sorbent which is functionalized with thiocyanate group to increase its selectivity that achieved the maximum binding capacity of 20.31 mg g^{-1} at pH 4.2 [29].

The present study is concerned with the preparation of crosslinked ion-imprinted polymer for Fe(II) ions while employing acrylic acid as a functional monomer, azobisisobutyronitrile as thermal initiator and acetonitrile

as solvent. The complexing agent of 1,10-phenanthroline is applied for coordination with the Fe(II) ions which will be later on used to functionalize the imprinted polymer. The as-prepared Fe(II) ion-imprinted polymer (IIP) will be used to adsorbed Fe(II) ions from the aqueous medium using ion-imprinted polymers.

2. Experimental

2.1. Chemicals and materials

Acrylic acid as a functional monomer, used for synthesis was hydroquinone monomethyl ether stabilized and was acquired from Sigma-Aldrich (Merck). N,N′-Methylenebis(acrylamide) having 99% purity was employed as a crosslinking agent and was procured from Sigma-Aldrich, Germany (Merck, Germany). Acetonitrile (anhydrous) with 99.8% purity was applied as a solvent for synthesis and azobisisobutyronitrile (AIBN) which was used as thermal initiator was obtained from Duksan Pure Chemicals, (South Korea). 1,10-phenanthroline with ≥99% purity was procured from Sigma-Aldrich (Merck) and was employed as a complexing agent for Fe(II) ions. Iron(II) chloride as anhydrous salt was also purchased from Sigma-Aldrich (Merck) with 99.99% purity. Glacial acetic acid having 99.7% purity was acquired from Alfa Aesar, Germany (Thermo Fisher Scientific, USA) for performing leaching. Commercial methanol was procured which was subjected to double distillation before use. Hydroxylammonium chloride with 98% purity was also purchased from Fisher Scientific, UK.

2.2. Instrumentation

In order to carry out the morphological analysis of the crosslinked polymer adsorbents, scanning electron microscopy (SEM) was applied to acquire the micrographs using a JEOL JSM-6300 (Japan). Similarly, for carrying out the infrared (vibrational) spectroscopy, PerkinElmer Spectrum 1000 (USA) Fourier-transform infrared (FTIR) spectrophotometer was employed with a resolution of 1 cm^{-1} using anhydrous KBr pellets to measure the infrared (IR) spectra in transmittance mode at room temperature. For performing the specific surface area analysis along with the surface texture analysis of the samples, N_2 adsorption isotherms were attained at liquid nitrogen temperature (77.350 K) employing the Quantachrome NOVA 2200e (USA). For removing the gases (N_2, O_2) and moisture that has been adsorbed at the sample's surface, they were also subjected to high vacuum drying at 70°C for 6 h in a vacuum oven prior to analysis. For performing the electrokinetic analysis in order to determine the electrokinetic parameters, Malvern Zetasizer Nano ZS (UK) was applied to record the electrostatic (zeta) ξ-potential at 25°C which employs the Laser (4 mW He-Ne laser at λ_{max} = 633 nm) doppler electrophoresis method applying the capillary cell with folded configuration provided with the gold electrode. An equilibration time of 10 min was set in place before measuring the data of electrophoretic mobility which was applied to calculate the electrostatic (zeta) ξ-potential using the following expression [30];

$$\xi = \frac{3\eta U_E}{2\varepsilon(\kappa\alpha)} \quad (1)$$

whereas U_E is the electrophoretic mobility, ε is the medium permittivity constant, η is medium's viscosity, 1/κ denotes the Debye length which is the statistically calculated electrical double layer thickness of ions present at the surface, α is the radius of the particle and $f(\kappa\alpha)$ represents Henry's function value, determined while assuming 1.5 value for Smoluchowski approximation on the basis of Smoluchowski model, for an aqueous medium which is polar having moderate electrolyte concentration [31]. Moreover, for evaluating the adsorbent's pH_{pzc} which depicts the pH that refers to the point of zero charge, 0.15 g L^{-1} adsorbent is used to prepare a colloidal suspension in the aqueous medium of deionized water which was subjected to ultrasonication for 20 min to attain the pH relaxation at the maximum that is adjusted by employing 10^{-2} M NaOH and HCl aqueous solutions. Centrifugation is carried to acquire the supernatant liquid which is then subjected to the electrostatic ξ-potential measurement. For measuring the absorbance of the tris(1,10-phenanthroline) Fe(II) complex, a UV-Visible spectrophotometer (HITACHI U-2900, Japan) was employed in the visible range of 400 to 600 nm. The maximum absorbance was recorded at 510 nm also referred to as λ_{max} for tris(1,10-phenanthroline) Fe(II) complex. The plot of peak absorbance against the Fe(II) ion concentration was subjected to linear regression from which a fitting equation was attained that was later on used to determine the concentrations of the unknown samples.

2.3. Iron(II) complex formation

The iron complex was prepared using 1,10-phenanthroline as a chelating ligand following the procedure described earlier [32]. For this purpose, 100 ppm solution of Fe(II) ions and 100 ppm solution of 1,10-phenanthroline were prepared. In order to attain maximum absorbance for stable tris(1,10-phenanthroline) Fe(II) complex, 3 mL of Fe(II) ions and 7 mL of 1,10-phenanthroline are mixed in a vial followed by adding 2 mL of 10 wt% of Hydroxylammonium chloride acidified with 0.01 M HCl and 3 mL of pH 4 buffer which was prepared by adding 100 mL of 5 M NaOH with 100 mL of 6 M CH_3COOH. The color of the tris(1,10-phenanthroline) Fe(II) complex was orange-red. Subsequently, the working standards of 20, 40, 60 and 80 ppm for Fe(II) ions were prepared from the stock solution and the above-mentioned procedure was followed to acquire the tris(1,10-phenanthroline) Fe(II) complex in each sample followed by absorbance measurement at λ_{max}. Furthermore, the unknown samples were also subjected to the same procedure as mentioned earlier followed by absorbance measurement which was eventually used in the fitting equation to determine the unknown concentration.

2.4. Preparation of non-imprinted polymer

The precipitation polymerization method was followed to synthesize the non-imprinted polymer [33]. The non-imprinted polymer was synthesized by adding 10 mL of acetonitrile as a solvent in a vial, 0.96 g acrylic acid as a functional monomer, 0.1 g N,N′-Methylenebis(acrylamide) as a cross-linker and 0.2 g AIBN was taken as a thermal initiator followed by heating at 90°C for 3 h in a water bath. The proceeding of the reaction was followed by observing

the appearance of white precipitates in the reaction mixture. Washing was performed through centrifugation where deionized water and methanol were used to wash the non-imprinted polymer followed by drying in an oven at 80°C for 24 h. Later on, the samples were crushed to powder in agate mortar and pestle.

2.5. Preparation of ion-imprinted polymer [Fe(II) IIP]

The preparation of imprinted polymer for Fe(II) ions follows the same procedure as mentioned above for the precipitation polymerization of the non-imprinted polymer but having an additional step which is the addition of complex as shown in Fig. 1. A vial was taken with 10 mL of acetonitrile, 0.96 g of acrylic acid and 0.1 g N,N′-Methylenebis(acrylamide) as a crosslinker which were mixed thoroughly to dissolve it completely. Then the tris(1,10-phenanthroline) Fe(II) complex which was attained by drying its solution at 60°C was also added to this solution followed by thorough stirring for 1 h to ensure homogeneous mixing. Afterwards, 0.2 g AIBN was taken as a thermal initiator and added to the solution which was placed in a water bath for 3 h at 90°C. The formation of white precipitate was observed which was used to monitor the proceeding of the precipitation polymerization reaction. Then, the precipitate was washed with 50% acetic acid aqueous solution followed by washing with deionized water and methanol and finally dried at 80°C for 24 h. The dried precipitates were then crushed to powder using agate mortar and pestle.

2.6. Equilibrium binding and kinetic studies

The equilibrium binding and kinetic studies were conducted in batch mode at four different temperatures (298, 323, 343, 363 K) in order to illustrate the adsorption isotherms, thermodynamic and kinetics parameters for both the non-imprinted polymer (NIP) as well as Fe(II) IIP [34]. In order to carry out this experiment, 0.05 g of the adsorbent was added to 5 mL of Fe(II) ions adsorbate solution with a different concentration in the range of 20 to 100 mg L^{-1} at neutral pH. For acquiring the dynamic equilibrium for the adsorbate adsorption on the adsorbent, an orbital shaker (MaxQ 7000) having a thermostatic water bath was employed for purpose of shaking at 110 rpm as shaking speed for 6 h. The centrifugation (Hettich MIKRO 220) was performed for 40 min at 11,000 rpm to separate the adsorbents from the adsorbate solution. It was followed by the determination of the Fe(II) ions concentration in the supernatant by applying the method elaborated in section 2.3. In order to perform the kinetic study for adsorption of Fe(II) ions on both the NIP and Fe(II) IIP at four different temperatures (298, 323, 343, 363 K), 0.05 g of each adsorbent is added to 5 mL separately having the Fe(II) ions solution with 100 mg L^{-1} concentration for a different time interval. The time variations for the kinetic study were 10, 30, 60, 120 and 180 min, respectively.

2.7. Selectivity studies

For elaborating the selectivity of the Fe(II) IIP, Fe(II) ions along with other metal ions (M) were competitively adsorbed on both the NIP as well as Fe(II) IIP by using their mixtures, respectively. The distribution coefficient denoted as the K_d (mL g^{-1}), k represented the selectivity coefficient, and the relative selectivity coefficient k' are given below as [33];

$$K_d = \frac{\left(C_0 - C_e\right)V}{C_e m} \tag{2}$$

$$k = \frac{K_{d\,\mathrm{Fe(II)}}}{K_{d\,(M)}} \tag{3}$$

$$k' = \frac{k_{(\mathrm{IIP})}}{k_{(\mathrm{NIP})}} \tag{4}$$

whereas the initial and equilibrium concentration of each metal ion in the solution is denoted as C_0 and C_e, respectively. The distribution coefficient of Fe(II) and M ions are denoted as $K_{d\,\mathrm{Fe(II)}}$ and $K_{d\,(\mathrm{M})}$ whereas the selectivity coefficient is represented as $k_{(\mathrm{IIP})}$ and $k_{(\mathrm{NIP})}$, respectively (M denotes the interfering metal ion).

3. Results and discussion

3.1. Scanning electron microscopy

The micrographs were attained by employing SEM in order to analyze the morphology of NIP and Fe(II) IIP adsorbents, respectively. As shown in Fig. 2, there is a difference visible in the morphology of NIP as compared to Fe(II) IIP. NIP adsorbents that were not subjected to imprinting displayed a layered and smooth appearance with irregularly shaped assembly showing a lack of homogeneity with respect to morphological profile as shown in Fig. 2a. In addition, the surface of the NIP adsorbent is also decorated with an agglomerate of small-sized beads with a diameter ranging from 100 to 500 nm along with irregularly shaped protrusions appearing at the surface. On the contrary, Fe(II) IIP adsorbent SEM micrograph shows non-uniform polydispersed shallow cavities with 100–1,000 nm diameter at the surface as this change can be attributed to imprinting at the adsorbent surface as shown in Fig. 2b. The topological profile for the Fe(II) IIP adsorbent show more rough appearance as compared to NIP adsorbent as the formation of surface cavities takes place due to imprinting that also leads to an increase in the specific surface area leading to an increase in the adsorption surface process pointing to the occurrence of interaction between the metal ion complex and polymer matrix.

3.2. Fourier-transform infrared spectroscopy

As the polymer backbone constituting the co-polymer of acrylic acid as functional monomer and N,N′-Methylenebis(acrylamide) as a cross-linker bears similarity in both the NIP and Fe(II) IIP adsorbent, therefore, the IR peaks in the spectrum show similarity due to similar molecular structure as shown in Fig. 3. The intrinsic peak of IR at 3,350 cm^{-1} corresponds to the stretching vibrations

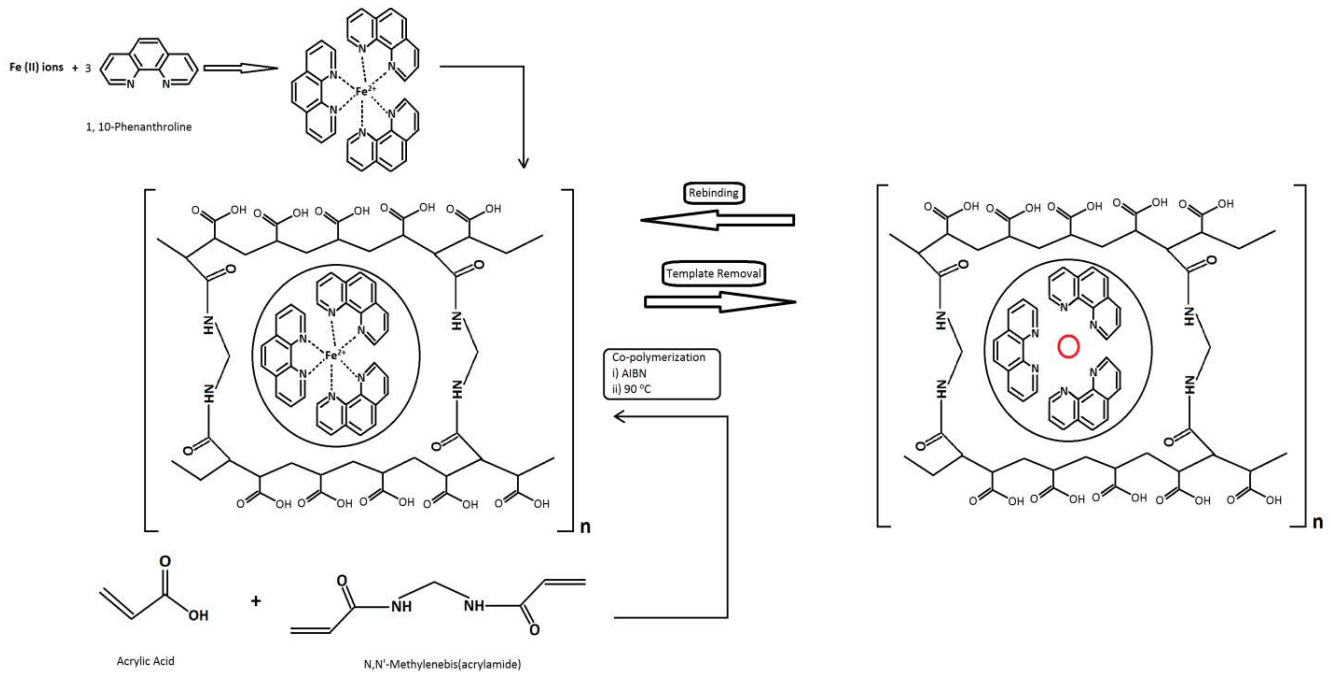

Fig. 1. Preparation of ion-imprinted polymer (IIP) [Fe(II) IIP].

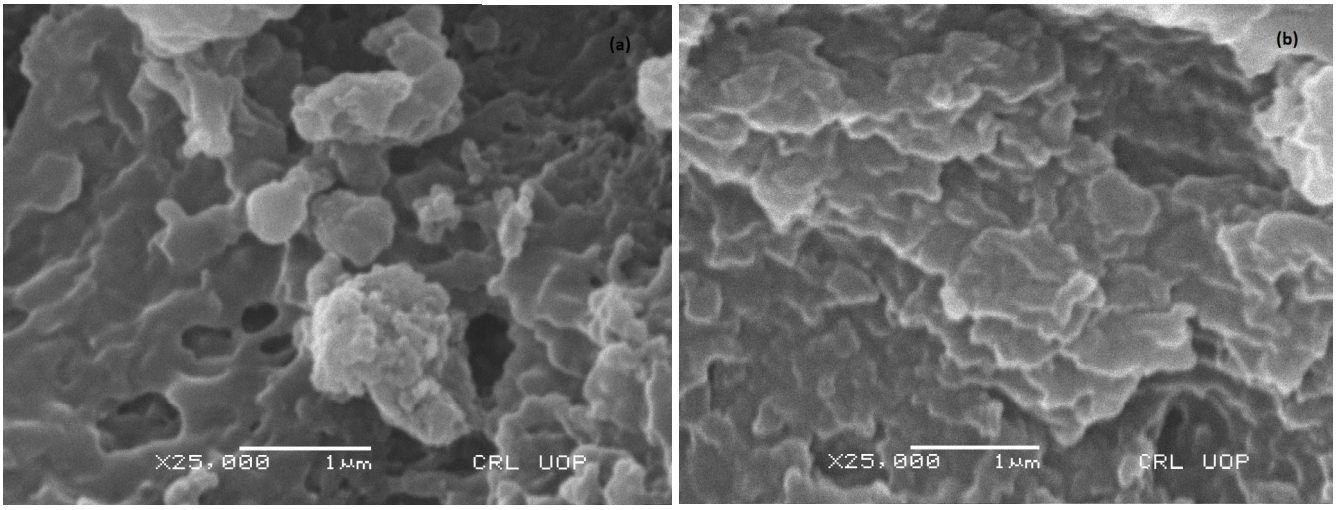

Fig. 2. SEM micrographs of (a) non-imprinted polymer (NIP) polymer and (b) Fe(II) ion-imprinted polymer (IIP) adsorbents.

of the amide (N–H) group for secondary amide whereas incase of the carbonyl (C=O) group having the stretching vibrations appears as a prominent peak at 1,682 cm^{-1} and the nitrile (C≡N) group have stretching oscillations with less prominent IR peak appearing at 2,244 cm^{-1} [35]. Similarly, the bending oscillations of the N–H group have been assigned peak appearing at 1,526 cm^{-1} [36]. The C–H group associated with methylene moieties of poly(acrylic acid-co-N,N′-Methylenebis(acrylamide) have a peak appearing at 2,948 cm^{-1}. IR peak at 1,655 cm^{-1} appearing as shoulder peak and 1,726 cm^{-1} assigned to the amide group and carboxyl group –COOH cause the shifting of the adsorption band associated with the C=O stretching vibration (1,682 cm^{-1}), depicting the strong nature of the hydrogen bonding occurring between –COOH and $–CONH_2$ [37]. In the case of Fe(II) IIP, the IR peaks appearing at 1,636, 1,518, 849 and 765 cm^{-1} corresponds to the C=C, C=N, C–H benzene ring and C–H pyridine ring for the Fe(II) ion coordinated with the 1,10-phenanthroline ligand [38]. The prominent peak appearing at 1,112 cm^{-1} corresponds to the stretching vibrations of C–O group at the C–O–Fe site [39]. The absence of IR peak at 1,630 cm^{-1} attributed to double bond stretching vibrations confirms the absence of the reactive vinyl group [36].

3.3. Surface area analysis

For the adsorbate concentrating at the porous surface in a stepwise manner, the proposed mechanism is of the

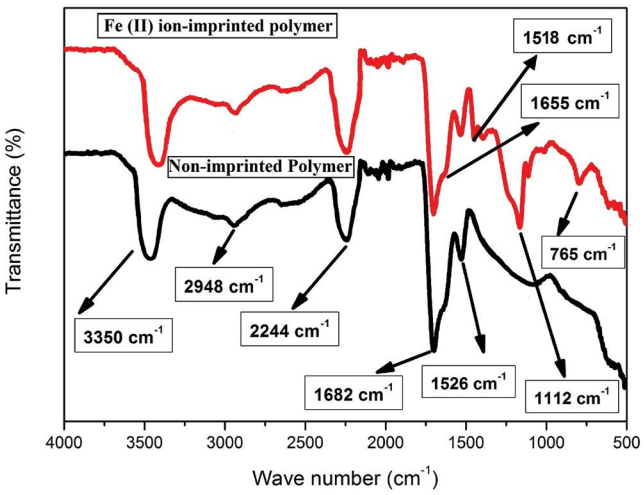

Fig. 3. FTIR spectrum of non-imprinted polymer (NIP) and Fe(II) ion-imprinted polymer (IIP).

capillary condensation also referred to as the pore-filling which is evident in the N_2 gas adsorption isotherms attained for NIP and Fe(II) IIP adsorbents as displayed in Figs. 4 and 5. Brunauer–Emmett–Teller (BET) isotherm depicting the model for the multilayer formation at the adsorbent surface is applied to N_2 gas adsorption isotherm which is then subjected to linear fitting below the recommended limit of relative pressure p/p^o in order to attain the specific surface area for the adsorbents;

$$\frac{1}{\left[Q\left(\frac{p^o}{p}-1\right)\right]}=\frac{c-1}{Q_m c}\left(\frac{p}{p^o}\right)+\frac{1}{Q_m c} \tag{5}$$

where Q is the adsorbed gas volume per unit mass of the respective adsorbent ($cm^3\ g^{-1}$), Q_m is the adsorbed gas volume for monolayer surface coverage ($cm^3\ g^{-1}$), p^o is the standard pressure, p is the equilibrium pressure and c is the factor that establishes the relationship of the heat of adsorption to the heat of liquefaction at a constant temperature [40]. The BET specific surface area attained for the NIP adsorbent is observed to be 473.44 $m^2\ g^{-1}$ as compared to 585.04 $m^2\ g^{-1}$ for Fe(II) IIP adsorbent which points to the fact that the increase in surface area can be contributed to the presence of the surface cavities due to imprinting resulting in an increase in the number of surface active sites available for adsorption.

The statistical thickness of the adsorbate accumulated at the surface of the adsorbent is attained using the de-Boer equation which is given as;

$$t\left(\text{Å}\right)=\left(\frac{13.99}{\log\left(\frac{p^o}{p}\right)+0.034}\right)^{1/2} \tag{6}$$

where t represents the adsorbed layer statistical thickness (Å) [41]. The t-plot is attained by plotting the volume of the N_2 gas which is adsorbed per adsorbent gram as a function of respective pressure against the thickness t (P). This plot gives an elaborative view of the porosity at the surface of the adsorbent in terms of the surface coverage at the pore internal and external surface. The linearity and non-linearity of the t-plot refer to the non-porous or porous surface of the adsorbent. The coverage by adsorbate at the internal as well as the external surface constitutes the total surface area when the adsorbent surface has a porous profile and can be attained from the t-plot region appearing prior to the capillary condensation when subjected to linear fitting. As the saturation of the capillary condensation is achieved resulting in the coverage of pore internal surface area, followed by the external surface area adsorption which can be used to attain the external surface area from the slope obtained after the linear fit of the t-plot region attributed to the external surface area coverage whereas the mesoporous volume area is provided by the intercept. Since these two regions are prominently evident in the t-plot which depicts the mesoporosity in the adsorbents. For NIP adsorbent, 0.369 $cm^3\ g^{-1}$ value of the mesopore volume is attained as compared to 0.418 $cm^3\ g^{-1}$ for Fe(II) IIP adsorbent which is a prominent increase. Similarly, when the external surface area is subtracted from the total surface area, the mesoporous surface area is attained which is found to be 318.55 $m^2\ g^{-1}$ for NIP adsorbent as compared to 442.67 $m^2\ g^{-1}$ for the Fe(II) IIP adsorbent. When in the low-pressure region of t-plot, if the linear fit does not pass through the origin, then it could lead to the pseudo assumption of the presence of the microporosity at the adsorbent surface as this method is valid for assessing the adsorption data if the size of the mesopores is 10 times in comparison to the size of the adsorbate molecule (N_2 molecule). Therefore, for large diameter mesopores, it is suitable to state that adsorption at the mesoporous surface will show behavior similar to the flat surface adsorption mechanism [42].

The lack of pore size narrow distribution is visible in the N_2 adsorption isotherm since the process of pore condensation is not outstanding. Therefore, Barrett, Joyner, Halenda (BJH) model is applied for evaluating the pore size in addition to the pore size distribution, to the N_2 adsorption isotherm for adsorption at 77 K when cylindrical pore shape is presumed (Area of pore = $A_p = 2V_p/r_p$) for completely describing the surface texture and subsequent equations for calculations are given as [43];

$$V_p = R_n \Delta V - R_n c \sum_{j=1}^{n-1} A_{pj} \tag{7}$$

$$R_n = \frac{r_p^2}{\left(r_k + \Delta t\right)^2} \tag{8}$$

$$c = \frac{\left(\overline{r_p} - t_r\right)}{\overline{r}_p} \tag{9}$$

$$\log \frac{p}{p^o} = \frac{-4.14}{r_k} \tag{10}$$

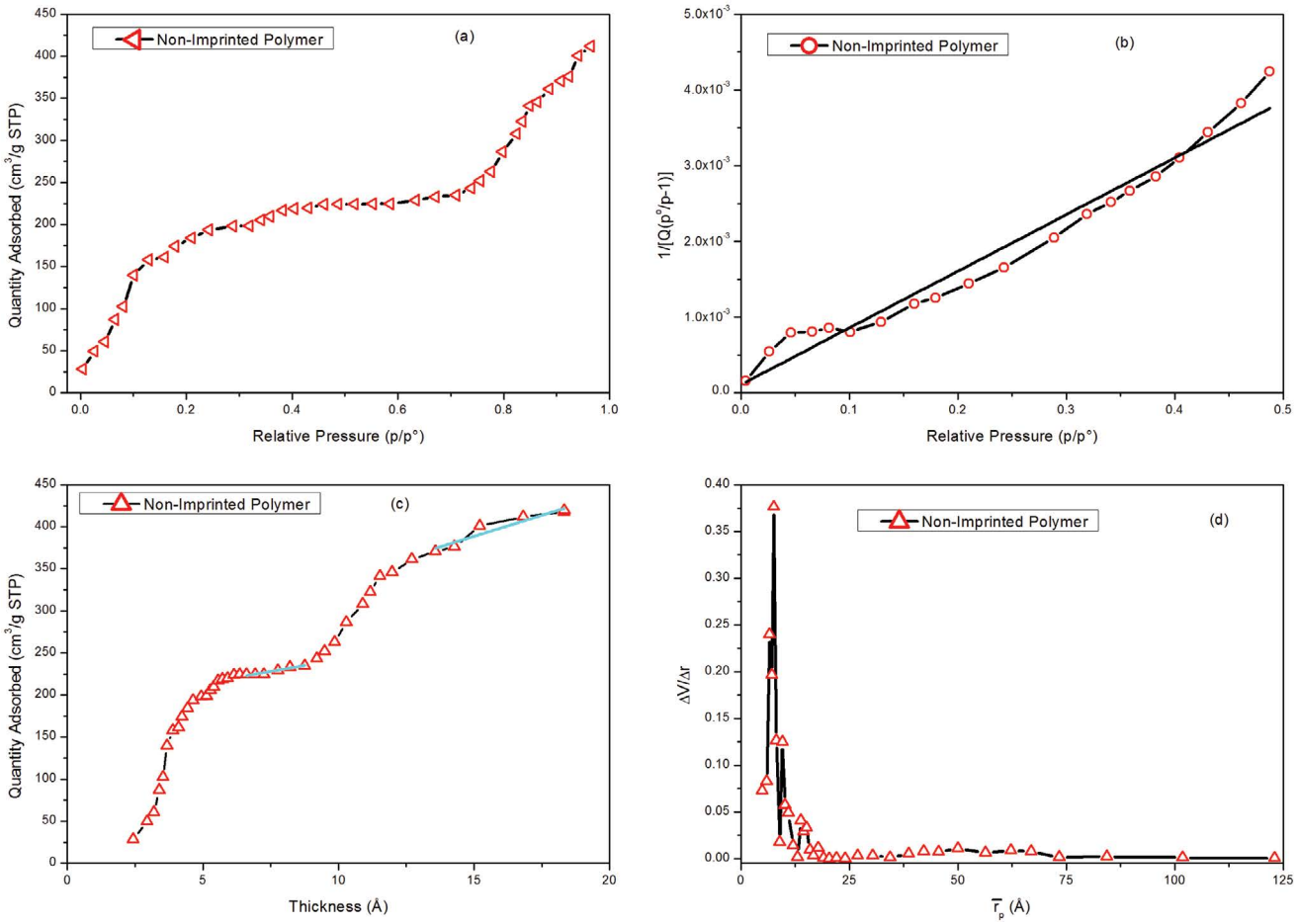

Fig. 4. (a) Nitrogen adsorption isotherm at 77 K, (b) BET surface area plot for nitrogen adsorption at 77 K with linear fitting, (c) *t*-plot model applied on nitrogen adsorption at 77 K with linear fitting, and (d) BJH model pore-size distribution for non-imprinted polymer (NIP) polymer.

whereas V_p denotes the pore volume, the desorbed gas volume is ΔV_p, empty pore radius is represented as r_p, inner capillary pore radius with physically adsorbed layer is given as r_k and the statistical thickness of the adsorbed layer is t_r. For NIP as well as Fe(II) IIP, the pore size is found to be greater than 4 nm pointing to the presence of the surface mesoporosity in both the polymer adsorbents respectively. The remaining physical parameters of the texture of the surface as obtained by the BET model and *t*-plot method are presented in Table 1.

3.4. Electrokinetic analysis

By using the theory of Gouy–Chapman, the estimation for the ionic specie concentration adjacent to the charged surface is achieved by applying the Boltzmann factor for attaining the total charge available per unit volume $\rho(x)$ as;

$$\rho(x) = \sum_i n_i^o z_i e \exp\left(\frac{-z_i e\xi}{kT}\right) \tag{11}$$

where the ionic specie concentration existing in the bulk is denoted as n_i^o, the valency of the ionic specie is represented as z_i, the electronic charge is e (C), k is the Boltzmann constant, electrostatic or zeta potential is denoted as ξ (mV) and T is the absolute temperature (K) [44].

Poisson Boltzmann equation for an electrolyte that is symmetrical is given as;

$$\frac{d\xi}{dx} = \left(\frac{8kTn^o}{\varepsilon\varepsilon_o}\right)^{1/2} \sinh\left(\frac{ze\xi}{2kT}\right) \tag{12}$$

It is apparent from the above-mentioned equation that the perturbation in the ξ zeta potential occurs as a function of the distance of the charged layer of accumulated ionic specie adjacent to the surface present in the diffuse layer. Since the charge density at the adsorbent surface σ^M is nearly equal to the charge density of the layer of ionic specie in solution phase in close proximity to the surface σ^S, therefore, a monotonic relationship is established between the charge per unit area $\sigma^M = q/A$ on the surface of the adsorbent and the zeta ξ potential as;

$$\sigma^M = -\sigma^S = \frac{q}{A} = \varepsilon\varepsilon_o\left(\frac{d\xi}{dx}\right) \tag{13}$$

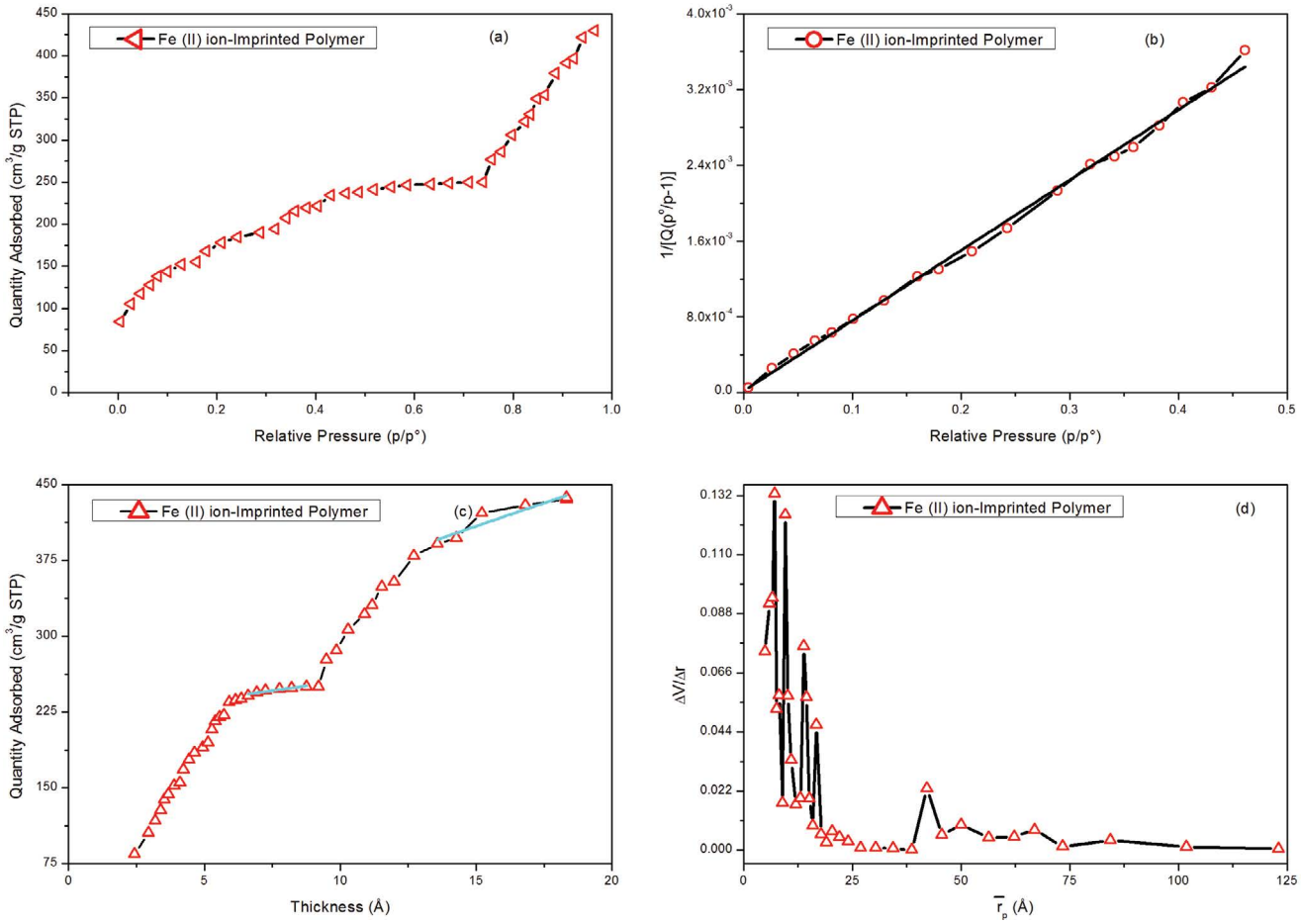

Fig. 5. (a) Nitrogen adsorption isotherm at 77 K, (b) BET surface area plot for nitrogen adsorption at 77 K with linear fitting, (c) *t*-plot model applied on nitrogen adsorption at 77 K with linear fitting, and (d) BJH model pore-size distribution for Fe(II) ion-imprinted polymer (IIP).

Table 1
Typical textural and surface parameters derived from N_2 adsorption at 77 K on non-imprinted polymer (NIP) and Fe(II) ion-imprinted polymer (IIP) using BET and *t*-plot models

Adsorbents	BET adsorption isotherm model				*t*-plot method				
	S_{BET} ($m^2\ g^{-1}$)	c	Q_m	R^2	$V_{Mesopore}$ ($cm^3\ g^{-1}$)	$S_{Mesopore}$ ($m^2\ g^{-1}$)	$S_{External}$ ($m^2\ g^{-1}$)	$S_{t\text{-plot}}$ ($m^2\ g^{-1}$)	R^2
NIP	473.44	68.92	131.75	0.95	0.37	318.45	154.55	0.02	0.96
Fe(II) IIP	585.04	379.55	134.41	0.98	0.42	442.37	142.67	0.02	0.99

$$\sigma^M = \left(8kT\varepsilon\varepsilon_o n^o\right)^{1/2} \sinh\left(\frac{ze\xi}{2kT}\right) \tag{14}$$

Eq. (14) is also referred to as the Grahame equation have the importance as it satisfies the electroneutrality criteria since the charge in the electrical double layer present in the solution phase and the surface charge becomes equal as displayed in Fig. 6b which elaborates the electrokinetic behavior of both the adsorbents [45]. In the same way, for the equality of the negative and positive charged sites present at the adsorbent surface, the attained state of electroneutrality is termed as the point of zero charge (pzc) at the adsorbent's surface corresponding to the zero surface charge density and is denoted as pH_{pzc} displayed in Fig. 6a. For the pH value below the pH_{pzc}, the positively charged sites at the adsorbent surface are abundant whereas, for values of pH greater than pH_{pzc}, the negatively charged sites are predominantly populated at the surface of the adsorbent which dually effects the adsorbent's zeta ξ potential at the surface with change in the pH as shown in Fig. 6a and b. The carboxyl group with a negative charge at the adsorbent surface is the most important reason for such electrokinetic behavior of the as-prepared adsorbents as such polymer

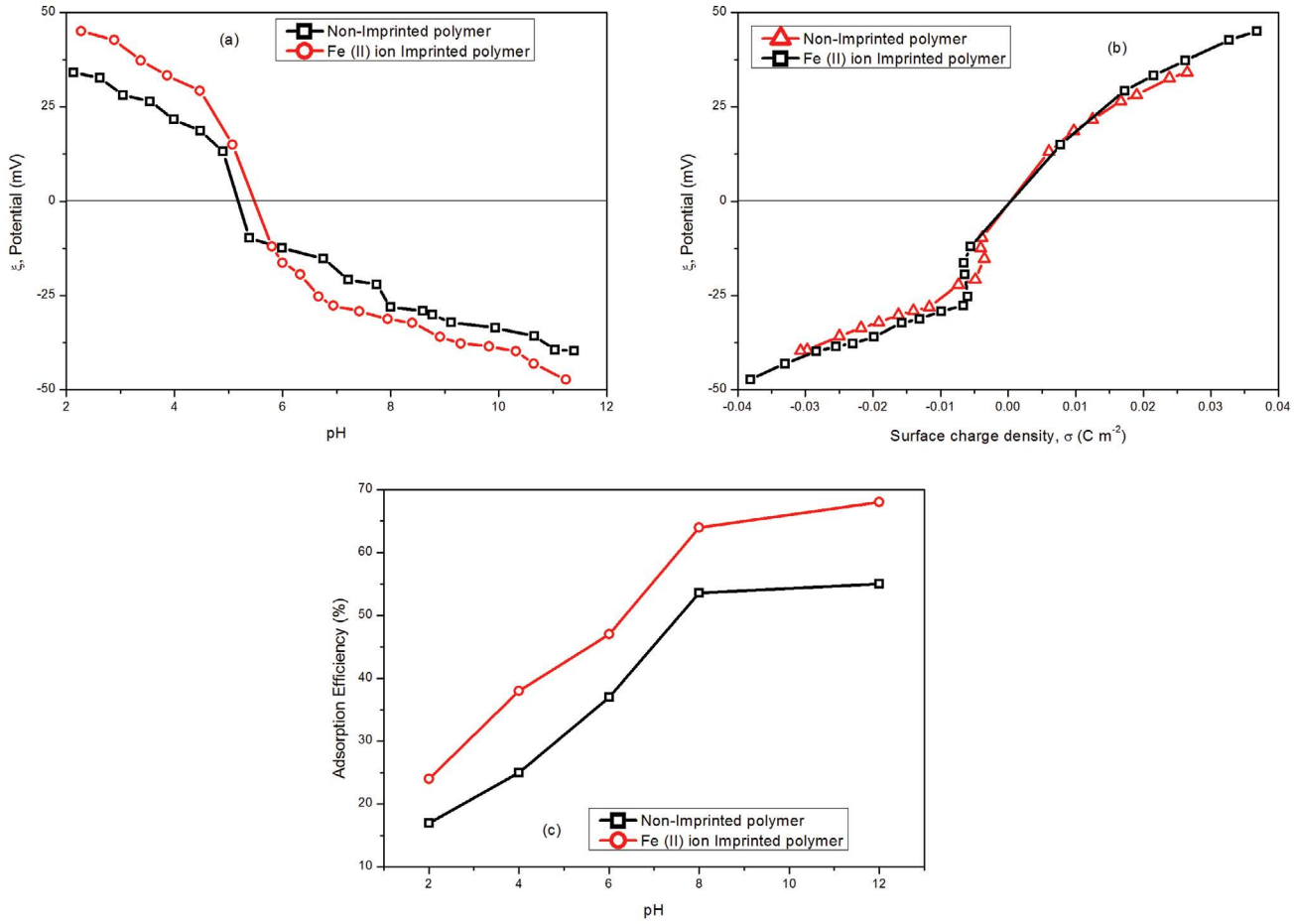

Fig. 6. (a) Point of zero charge pH_{pzc} measurement, (b) surface potential vs. surface charge, and (c) depicts the influence of pH on the adsorption of Fe(II) ions on adsorbents.

segments having –COOH groups cause an increase in the surface charge density σ value since the pH change affects the carboxyl group dissociation at the surface of the polymer adsorbent. On the contrary, the presence of the structure of the tail and loop of the polymer segments at the surface add to the decrease in the σ value. Therefore, it can be stated that the value of σ which is attained empirically comprises of both these effects [46]. The H^+ ions adsorption at the adsorbent surface due to carboxyl group which acts as a proton donor and acceptor also result in shifting of the zeta ξ potential with respect to pH change as the carboxyl group are protonated at lower pH due to basic nitrogen causing an increase whereas the deprotonation at higher pH results in lowering of the zeta ξ potential [47,48]. The higher value of the ξ potential for Fe(II) IIP as compared to NIP can be attributed to the presence of additional molecular moieties pertaining to the 1,10-phenanthroline presence which also undergoes protonation or deprotonation as it causes the dissociation or formation of 1,10-phenanthroline complexes and it can also be associated to the decrease in the zeta ξ potential value with the increase in the pH value such as the 1,10-phenanthroline is present as phenanthrolium ion at lower pH [49]. As given in Fig. 6a, the pH_{pzc} is 5.1 for NIP as compared to 5.5 for Fe(II) IIP, respectively.

The change in pH has a pronounced affect on the electrokinetic parameters of the polymer adsorbents as the molecular groups exposed at the surface to the medium will undergo a change in their respective ionic state according to the change in pH of the solution. As the negative charge increases at the adsorbent surface with the increase in the pH value which lead to the formation of the positively charged Fe(II) ions complex with the active surface sites of adsorbent as a result of the electrostatic attractive forces causing an increase in the adsorption efficiency as displayed in Fig. 6c. On the contrary, the electrostatic forces of repulsive nature are outstanding between adsorbent and adsorbate at the values of pH above pH_{pzc} [50].

3.5. Adsorption equilibrium studies

The expression for calculating the adsorption efficiency is given below as [51];

$$\text{Adsorption Efficiency} = \frac{C_o - C_e}{C_o} \times 100 \tag{15}$$

where C_o is the initial adsorbate concentration while C_e is the equilibrium adsorbate concentration (mg L^{-1}). The plot

of adsorption efficiency against the initial adsorbate concentrations for the adsorption of Fe(II) ions on both NIP and Fe(II) IIP adsorbent at four different temperatures (298, 323, 343 and 363 K) is attained as shown in Fig. 7a and b with the standard deviation for adsorption efficiency values listed in Table 2. It is apparent in Fig. 7a for NIP adsorbent that there are vacant sites at adsorbent surface available for adsorbate to occupy at the initial stage of adsorption process due to which the adsorption efficiency rapidly increases at low adsorbate concentration but eventually become steady indicating the occupation of surface active sites by adsorbate ions at higher concentration. Alternatively, it can also be suggested that no more active sites are available for the adsorption of Fe(II) ions after achieving the equilibrium. The adsorption efficiency of Fe(II) ions adsorption on Fe(II) IIP as displayed in Fig. 7b shows a similar behavior with greater adsorption efficiency in contrast to NIP due to the presence of more surface-active sites occurring due to imprinting as 1,10-phenanthroline is incorporated as a chelating agent in the cross-linked polymer adsorbent [52]. The temperature effect on adsorption efficiency is not very apparent but on average the adsorption efficiency increases with the temperature increase indicating that the adsorption affinity of both NIP and Fe(II) IIP towards Fe(II) ions is of endothermic nature [53]. The increase in the specific surface area can be attributed to the imprinting process that results in an increase in mesoporosity which contributes to an increase in the Fe(II) ions adsorption efficiency on Fe(II) IIP [54].

Table 2
Standard deviation analysis for the adsorption of Fe(II) ions on non-imprinted polymer (NIP) and Fe(II) ion-imprinted polymer (IIP) at different temperatures

Adsorbents	T (K)	Standard deviation (SD)	
		Adsorption efficiency	Adsorption isotherm
NIP	298	2.54	1.39
	323	33.14	1.82
	343	11.38	1.36
	363	22.63	2.80
IIP	298	22.95	2.07
	323	19.15	1.22
	343	9.50	2.06
	363	18.42	2.76

The plot of q_e denoting the adsorption capacity against the adsorbate equilibrium concentration C_e at four different temperatures display the adsorption isotherm as shown in Fig. 8a and b, is significant for evaluating the Fe(II) ions adsorption mechanism on NIP and Fe(II) IIP as adsorbent with the standard deviation for q_e values listed in Table 2.

The equation applied for determining the adsorbent adsorption capacity is as follows:

$$q_e = \frac{\left(C_o - C_e\right)V}{m} \tag{16}$$

where q_e is the adsorption capacity of Zn(II) ions on adsorbent (mg g^{-1}), V is the volume of Zn(II) ion solution (L) and m is the mass of adsorbent used (g). It is apparent from the plot that there is a prominent increase in the adsorption capacity due to the initial adsorbate concentration increase until the saturation is achieved indicated by a region of semi-plateau in the plot. Furthermore, with the rise in temperature, the adsorption capacity tends to increase indicating the endothermic nature of the adsorption phenomenon. For Fe(II) IIP adsorbent, the value achieved for the maximum adsorption capacity was greater as compared to the NIP adsorbent that can be attributed to the mesoporosity in the adsorbent as elaborated due to imprinting, respectively. Moreover, high temperature favors the Fe(II) ions adsorption on both the adsorbent due to endothermic nature which results in capturing of the

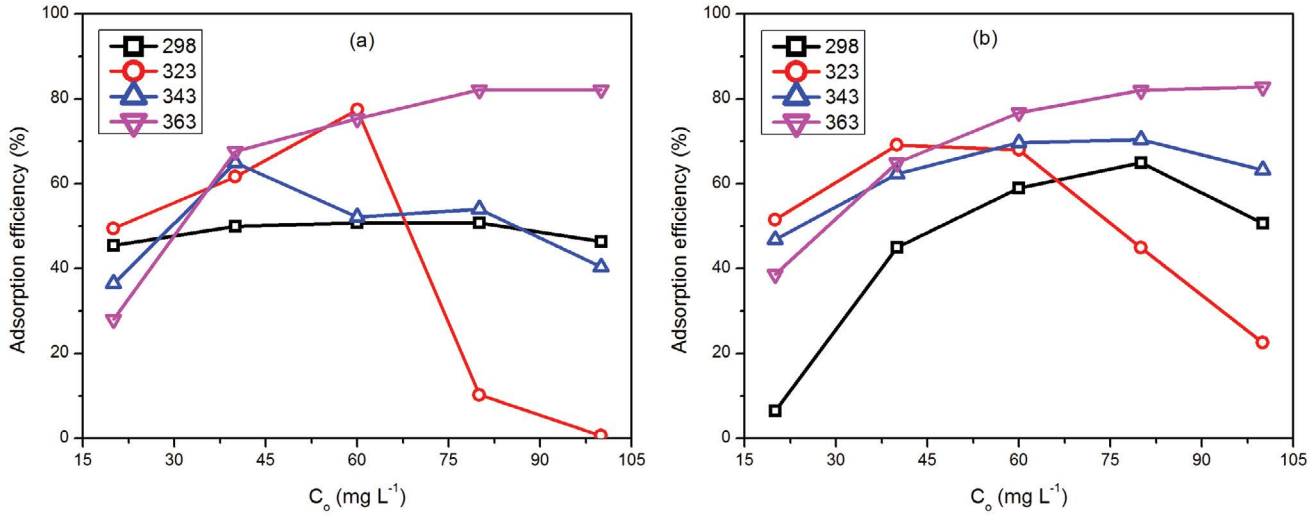

Fig. 7. Percent adsorption efficiency of adsorption of Fe(II) ions on (a) non-imprinted polymer (NIP) and (b) Fe(II) ion-imprinted polymer (IIP) adsorbent at pH = 7.

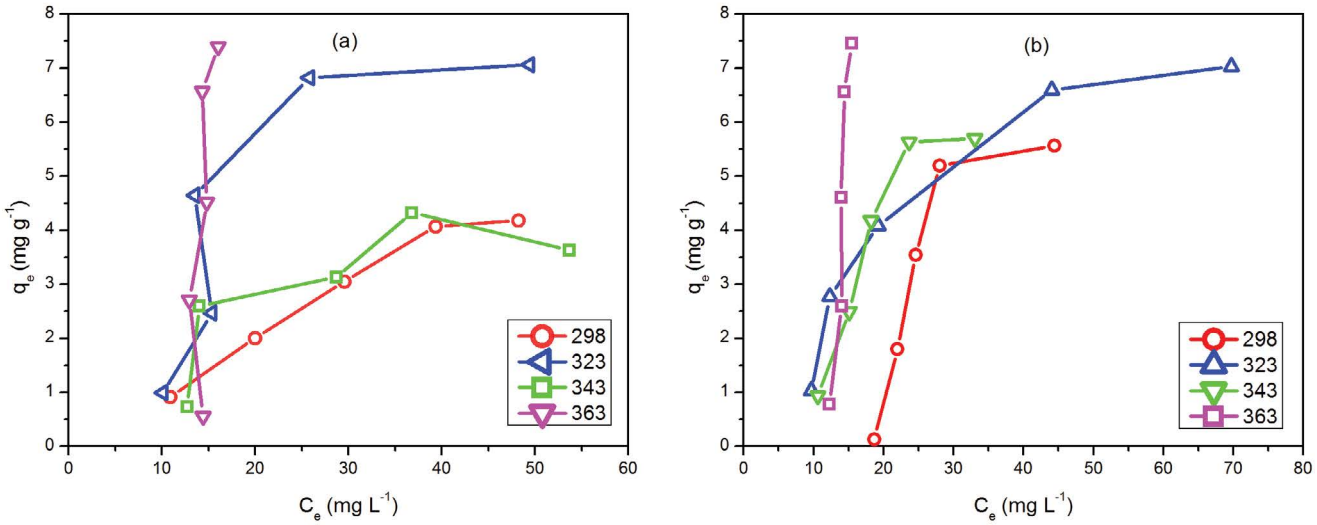

Fig. 8. Adsorption isotherm plot of q_e vs. C_e for the equilibrium adsorption data of adsorption of Fe(II) ions on (a) non-imprinted polymer (NIP) and (b) Fe(II) ion-imprinted polymer (IIP) adsorbent at pH = 7.

Fe(II) ions from the liquid to solid phase corresponding to an increase in the strength of the adsorptive and thermodynamic driving forces. Hence, the phenomenon of physical adsorption is accompanied by chemical adsorption pertaining to low heat of adsorption [55]. The chelating agent of 1,10-phenanthroline has an electron-withdrawing group which is incorporated in Fe(II) IIP that chelates with Fe(II) ions resulting in the Fe(II) ions complementary cavities in the IIP adsorbent whereas on the other hand, the chelating groups of –NH and –COOH are present in the NIP adsorbent for chelation.

The equilibrium adsorption data, when subjected to linear fitting with straight-line equations of different models of adsorption isotherm such as Langmuir, Freundlich, Dubinin–Radushkevich and BET model give parameters that carry significance for illustrating the mechanism of the adsorption.

The identical surface sites, when occupied with the respective adsorbate leading monolayer formation are the basic fundamental assumption for the Langmuir isotherm model elaborating the non-porous surface homogeneity. The empirical equation of Langmuir in its linear form is given as;

$$\frac{C_e}{q_e} = \frac{1}{q_o K} + \frac{C_e}{q_o} \tag{17}$$

where C_e represents the equilibrium concentration of solute (mg L^{-1}), q_e represents the equilibrium solid-phase adsorption capacity (mg g^{-1}), K is the equilibrium adsorption constant (L mg^{-1}) and q_o illustrates the adsorbent maximum monolayer adsorption capacity (mg g^{-1}) [56]. The values of K and q_o were attained from the value of the intercept $1/q_oK$ and slope $1/q_o$ obtained after linear regression on the straight-line plot of C_e/q_e against C_e, respectively as shown in Fig. 9a and b. The NIP adsorbent at 323 K showed 0.07 mg g^{-1} value for the maximum monolayer adsorption capacity q_o as compared to 2.27 mg g^{-1} for the Fe(II) IIP suggesting the enhancement in adsorption capacity as a signature of more efficiency of Fe(II) IIP for Fe(II) ions adsorption. Furthermore, the maximum monolayer adsorption capacity q_o attained in the present study for Fe(II) IIP adsorbent for adsorption of Fe(II) ions is comparable with respect to the earlier work carried out reporting a value of 28.30 mg g^{-1}, respectively [33]. Therefore, it can be suggested that the imprinting method has produced a prominent effect on the adsorption efficiency of the adsorbent due to the successful creation of imprinted cavities at the adsorbent surface after leaching as a result of enhanced compatibility of the 1,10-phenanthroline-chelate complex with the polymer matrix that can be potentially employed for separation of metal ions [53].

In the case of adsorbents with surface porosity, then there is the existence of heterogeneous surface sites having different affinities for adsorbate adsorption at the adsorbent surface. Therefore, the Freundlich adsorption isotherm model assumes that active surface sites with more affinity are predominantly occupied by adsorbate species followed by adsorption at low-affinity surface sites [57]. Moreover, as the adsorbate concentration increases, the surface-active sites are occupied which leads to a gradual decrease in the adsorption capacity [58]. The empirical equation of the Freundlich isotherm is given in its linear logarithmic form as;

$$\ln q_e = \ln K_f + \left(\frac{1}{n}\right)\ln C_e \tag{18}$$

where q_e is the Fe(II) ions adsorption capacity (mg g^{-1}) of the adsorbent at equilibrium, C_e is the equilibrium concentration of adsorbate, $1/n$ is the adsorption index also known as the non-linearity exponent and K_f represents the Freundlich adsorption constant depicting the adsorption capacity (mg g^{-1})/(L mg^{-1}). The values of K_f and $1/n$ were calculated by the intercept and slope of the linear plot of $\ln q_e$ against $\ln C_e$ as shown in Fig. 10a and b, respectively [59]. When the values of K_f are high, the adsorption process

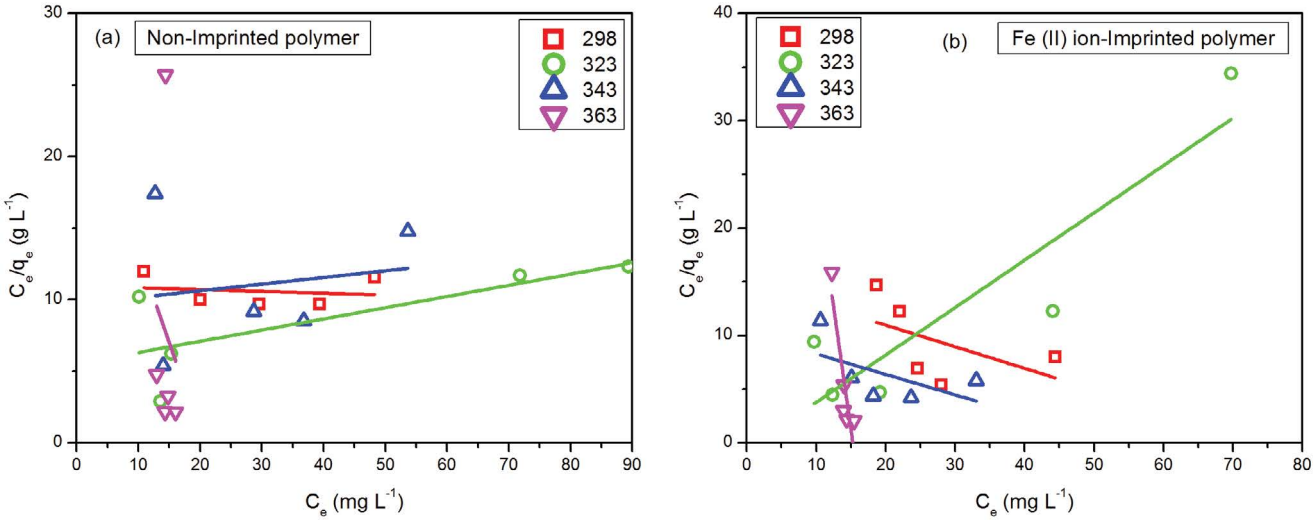

Fig. 9. Equilibrium adsorption data fitted with Langmuir adsorption isotherm model for adsorption of Fe(II) ions on (a) non-imprinted polymer (NIP) and (b) Fe(II) ion-imprinted polymer (IIP) adsorbent.

occurs significantly and it increases with the rise in temperature depicting the increase in adsorption pertaining to the endothermic nature [60,61]. For the value of $1/n$ less than 1, the adsorbate tends to show strong interaction with the adsorbent favoring the adsorption process whereas for an increase in the value of $1/n$, the adsorption process is favored to a lesser extent as the dependency of the q_e decreases on the C_e causing an enhancement in the adsorption process [62]. At higher temperature, the $1/n$ values are lower corresponding to the better adsorption due to the endothermic nature for the Fe(II) ions adsorption on NIP and Fe(II) IIP adsorbent.

The parameters derived from the Langmuir and Freundlich adsorption isotherms are listed in Table 3, from which it is evident that correlation coefficient R^2 for Freundlich isotherm applied on equilibrium adsorption data of Fe(II) ions adsorption on NIP and Fe(II) IIP is in the range of 0.12–0.98 and 0.11–0.88 respectively, which are greater in comparison to the values of R^2 for Langmuir isotherm which is also employed, pertaining to the fact that the Fe(II) ions adsorption more closely follows the Freundlich adsorption isotherm pointing to the heterogeneity of the adsorbent surface [63].

Dubinin–Radushkevich isotherm in its linear logarithmic form is given as;

$$\ln q_e = \ln q_m + K'\varepsilon^2 \tag{19}$$

where q_e represents the adsorption capacity at equilibrium (mg g^{-1}), q_m denotes the adsorbent maximum monolayer adsorption capacity (mg g^{-1}) while considering the microporous texture of the surface [64], ε is the Polanyi potential and K' is the adsorption energy constant (mol^2 kJ^{-2}) [65]. The value of K' and q_m are attained from the slope and intercept of the straight-line plot of $\ln q_e$ against ε^2 as displayed in Fig. 11a and b. Polanyi potential ε illustrates the influence of temperature on the adsorption process by employing the equilibrium concentration C_e (mg L^{-1}) of adsorbate in the following form given:

$$\varepsilon = RT\ln\left(1+\frac{1}{C_e}\right) \tag{20}$$

where R is the universal gas constant. The decrease in the value of C_e leads to an increase in the ε values results in an increase in the adsorption efficiency. The mean adsorption energy E (kJ mol^{-1}) derived using the adsorption energy constant K' value explores the chemical or physical nature of adsorption and is given as:

$$E = \frac{1}{\left(2K'\right)^{\frac{1}{2}}} \tag{21}$$

For the occurrence of the physical adsorption, E < 8 kJ mol^{-1}, whereas on the other hand, E = 8–16 kJ mol^{-1} depicts the adsorption to be of chemical nature, respectively [66]. The values of E for the Fe(II) ions adsorption on both the NIP and Fe(II) IIP adsorbents, points to the fact that the adsorption of physical nature has occurred pertaining to the monolayer formation since the adsorbent surface active sites chelate with the adsorbate. The rise in temperature results in the increase in the E values that affirms the endothermic nature of adsorption.

For Fe(II) ions adsorption at the surface of adsorbents in the solution phase, the multilayer model BET for the adsorption can be applied in the linear form given as:

$$\frac{C_e/C_o}{q_e\left(1-\frac{C_e}{C_o}\right)} = \frac{1}{q_x C} + \frac{C-1}{q_x C}\frac{C_e}{C_o} \tag{22}$$

where C_o represents the initial adsorbate concentration (mg g^{-1}), C_e denotes the Fe(II) ions concentration at equilibrium (mg L^{-1}), q_e is the adsorbent adsorption capacity at the equilibrium (mg g^{-1}), q_x is the adsorption capacity for monolayer formation and C is the constant factor illustrating the

Table 3
Values of various applied adsorption isotherm model parameters for adsorption of adsorption of Fe(II) ions (a) non-imprinted polymer (NIP) and (b) Fe(II) ion-imprinted polymer (IIP) adsorbent at different temperatures

Adsorption isotherm equation		Langmuir		
Adsorbent	T (K)	q_o (mg g^{-1})	K (L mg^{-1})	R^2
NIP	298	–78.13	–0.001	0.03
	323	0.07	–0.06	0.59
	343	21.50	0.01	0.03
	363	–0.80	–0.05	0.02
IIP	298	–0.33	–0.03	0.25
	323	2.27	–0.69	0.83
	343	–5.26	–0.02	0.32
	363	–0.22	–0.07	0.81
Adsorption isotherm equation		Freundlich		
Adsorbent	T (K)	K_f [(mg g^{-1})/(L mg^{-1})]	$1/n$	R^2
NIP	298	0.08	1.06	0.98
	323	52.10	1.25	0.57
	343	0.15	0.87	0.58
	363	0.00001	4.79	0.12
IIP	298	0.00002	3.50	0.54
	323	1.21	0.22	0.11
	343	0.03	1.61	0.84
	363	4.72×10^{-12}	10.35	0.88
Adsorption isotherm equation		Dubinin–Radushkevich		
Adsorbent	T (K)	k' (mol^2 kJ^{-2})	E (kJ mol^{-1})	q_m (mg g^{-1})	R^2
NIP	298	-3.20×10^{-05}	0.13	4.08	0.93
	323	-2.11×10^{-05}	0.15	5.21	0.01
	343	-2.93×10^{-05}	0.13	4.54	0.61
	363	-5.53×10^{-05}	0.10	30.95	0.19
IIP	298	-1.22×10^{-01}	0.07	9.38	0.76
	323	-1.28×10^{-05}	0.20	3.46	0.28
	343	-3.28×10^{-05}	0.12	8.11	0.98
	363	-1.19×10^{-04}	0.07	619.76	0.87
Adsorption isotherm equation		BET		
Adsorbent	T (K)	C	q_x (cm^3 g^{-1})	R^2
NIP	298	–1.14	0.16	0.25
	323	–1.65	0.001	0.43
	343	–1.60	0.28	0.32
	363	–3.62	0.15	0.95
IIP	298	–1.28	0.01	0.93
	323	–2.56	0.45	0.73
	343	–2.29	0.29	0.87
	363	–3.88	0.28	0.92

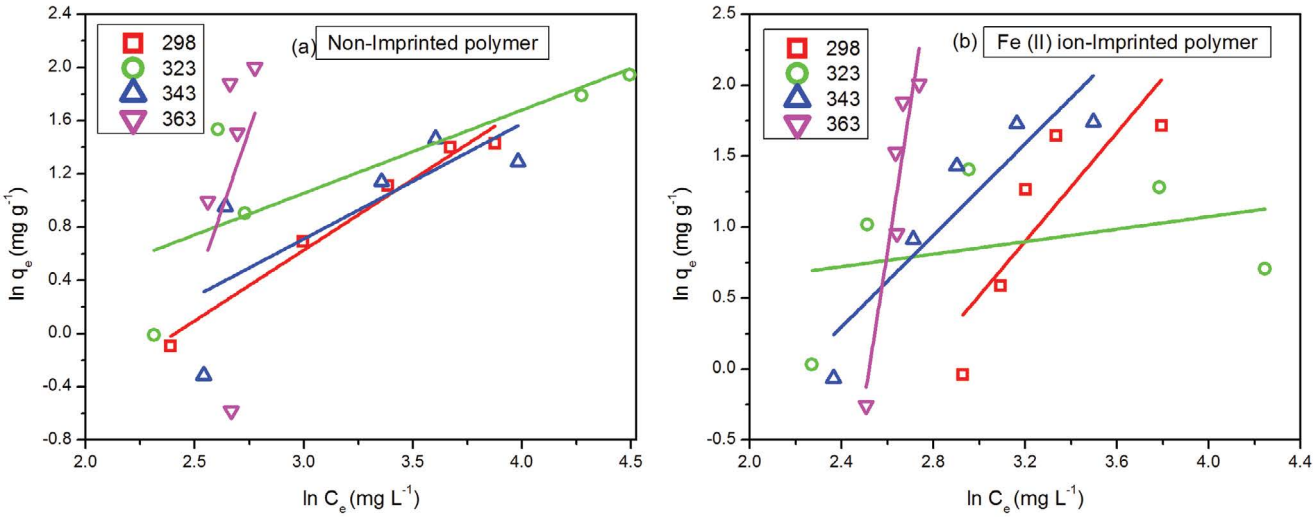

Fig. 10. Equilibrium adsorption data fitted with Freundlich adsorption isotherm model for adsorption of Fe(II) ions on (a) non-imprinted polymer (NIP) and (b) Fe(II) ion-imprinted polymer (IIP) adsorbent.

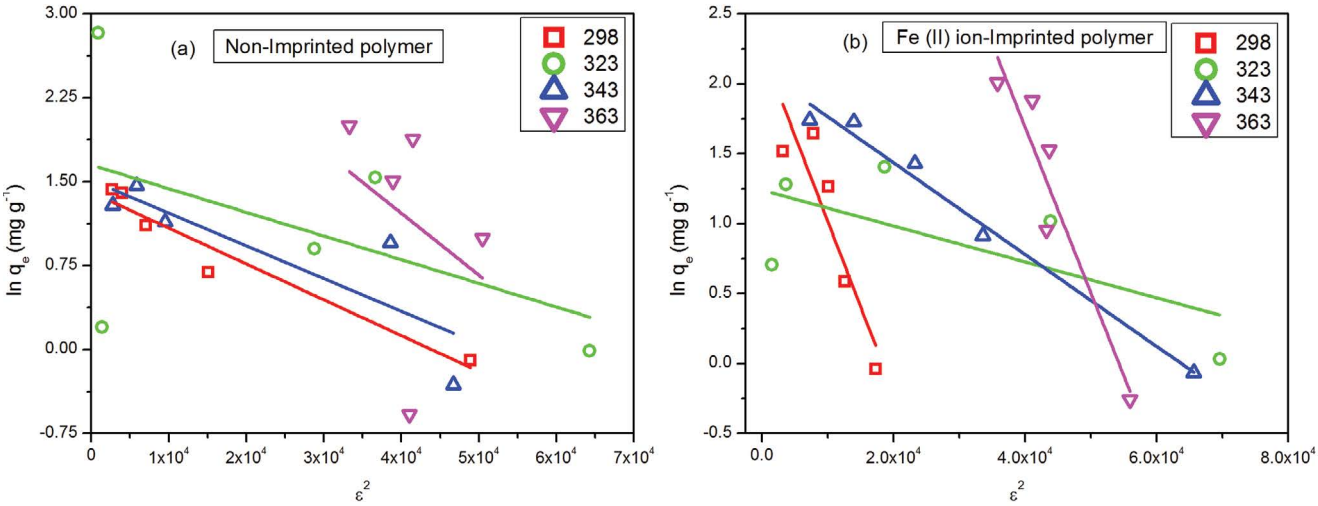

Fig. 11. Equilibrium adsorption data fitted with Dubinin–Radushkevich adsorption isotherm model for adsorption of Fe(II) ions on (a) non-imprinted polymer (NIP) and (b) Fe(II) ion-imprinted polymer (IIP) adsorbent.

energy relationship between the adsorbate and the adsorbent and is given as [67];

$$C = e^{(E_1 - E_L)/RT} \tag{23}$$

where E_1 and E_L represent the heat of adsorption for the adsorption of the first layer and second adsorbate layer. From the plots, as shown in Fig. 12a and b, the linearity decreases with the increase in temperature for adsorption of Fe(II) ions on NIP as compared to Fe(II) IIP for which the linearity of the BET plot increases depicting multilayer formation of the adsorbate at high temperature. As the adsorbent surface, active sites have a high affinity for Fe(II) ions adsorption due to which the heat of adsorption E_1 for the adsorbate first layer adsorption is high resulting in an increase in the C value at higher temperature [68].

Ion imprinting technique was applied for the removal of Fe^{3+} ions which were produced imprinted polymers with an average size of 63 to 140 μm via suspension polymerization and observed the maximum binding capacity to be 107 μmol g^{-1} at pH 3.0 whereas the equilibrium binding time was 30 min. Similarly, the efficacy of selective extraction was 97% even in the presence of many other ions in the solution [69]. A novel ion-imprinted polymer (IIP) for the extraction of Pb^{2+} was synthesized using the methacrylic acid and vinyl pyridine as dual-functional monomer based on ionic interactions and employing ethylene glycol dimethacrylate as cross-linker [70]. It was observed that the IIPs exhibited significant selectivity toward Pb^{2+} in presence of other divalent metal ions of Cu^{2+}, Cd^{2+}, Zn^{2+}, and Mn^{2+} showing selectivity coefficients greater than 30, as well as achieving 0.06 and 0.19 μg L^{-1} as the limits of detection and quantification. Fe(III) imprinted

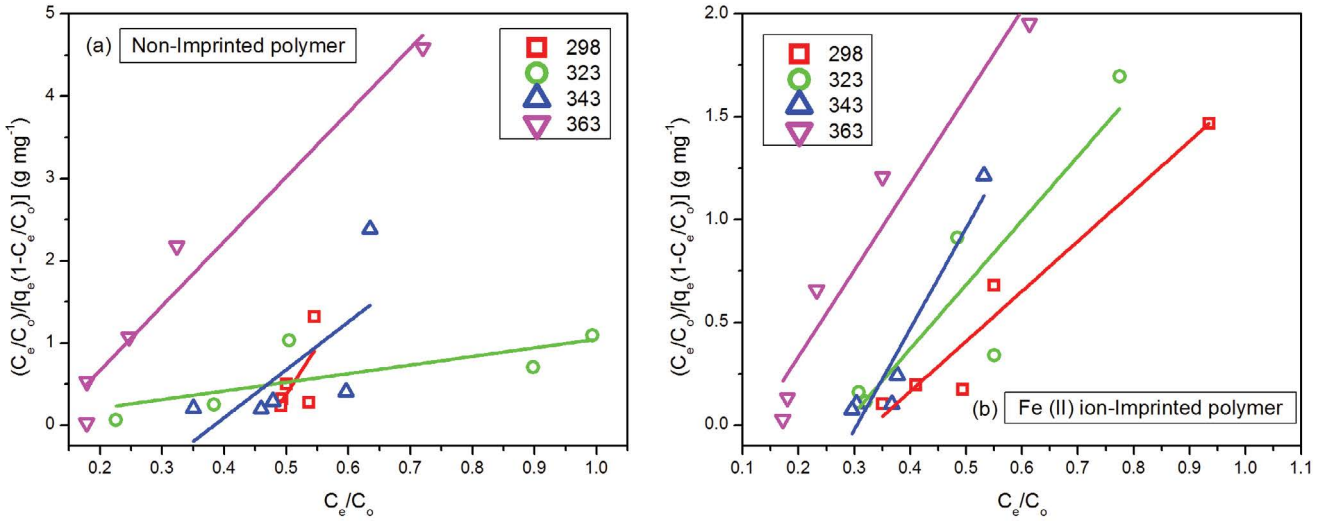

Fig. 12. Equilibrium adsorption data fitted with BET adsorption isotherm model for adsorption of Fe(II) ions (a) non-imprinted polymer (NIP) and (b) Fe(II) ion-imprinted polymer (IIP) adsorbent.

amino-functionalized silica gel adsorbent was prepared which was successfully used for the extraction of trace metal Fe(III) through solid-phase extraction technique [14]. The adsorption capacity for adsorption of Fe(III) was found to be 25.21 mg g^{-1} for the IIP while 5.10 mg g^{-1} for NIP. A facile and sensitive procedure was developed for the selective extraction of ferric ion (Fe^{3+}) from the aqueous medium by preparing an imprinted resin with different amount of crosslinkers ranging from 85 to 3 mol%. It was observed that a larger adsorption capacity for Fe^{3+} was attained for the resin having a high amount of crosslinking but it was also found to be lower in selectivity [71]. Similarly, a multiwalled carbon nanotubes column for the preconcentration of certain ions such as Cu^{2+}, Pb^{2+}, Mn^{2+} and Fe^{3+} was developed for their solid-phase extraction for which at pH 9.0, the quantitative adsorption was achieved with a preconcentration factor of 20 and detection limits in the range of 3.5 to 8.0 μg L^{-1} [72]. An ion-imprinted polymer (IIP) with monophosphonic groups was prepared using bis(2-methacryloxyethyl) phosphate (BMAOP) as a functional monomer to chelate with Fe^{3+} in dimethyl sulfoxide (DMSO) medium and ethylene glycol dimethacrylate (EGDMA) as cross-linker during thermal polymerization which showed that the monophosphonic groups could be selectively combined with Fe^{3+} in solutions containing other interfering metal ions [73].

3.6. Adsorption thermodynamics

The change in the Gibbs free energy (ΔG), entropy (ΔS), and enthalpy (ΔH) are the parameters of thermodynamics used in order to study the equilibrium adsorption process of Fe(II) ions on both NIP as well as Fe(II) IIP with respect to temperature. For evaluating the thermodynamic parameters, Van't Hoff equation is applied which integrates the absolute temperature (T) to the adsorption equilibrium constant (K) that is attained from the Langmuir adsorption isotherm model respectively. The logarithmic linear Van't Hoff expression is given as [74];

$$\ln K = \left(\frac{\Delta S}{R}\right) - \left(\frac{\Delta H}{RT}\right) \tag{24}$$

The slope and intercept of the linear plot of ln$K$ vs. 1/T as shown in Fig. 13, is used to find the change in enthalpy (ΔH) and entropy (ΔS) respectively, whereas Gibbs free energy change (ΔG) is determined by the equation given below as [75];

$$-\Delta G = -\Delta H + T\Delta S \tag{25}$$

At equilibrium, ΔG as the driving force is related to the adsorption equilibrium constant K as the standard Gibbs free energy change ΔG_o is inherently equal to zero and ΔG is given at equilibrium by the following equation as;

$$\Delta G = -RT\ln K \tag{26}$$

So according to the calculated values of the thermodynamic parameters as shown in the Table 4 for both NIP as well as Zn(II) IIP, ΔH values are negative indicating the exothermic nature of adsorption for the adsorption of Fe(II) ions [76]. The positive value for entropy change (ΔS) suggests that there is no thermodynamic barriers for the Fe(II) ions adsorption on adsorbent indicating the spontaneous nature of adsorption which cause an increase in the randomness of the adsorption process [77]. The negative value of ΔG suggests that the spontaneous adsorption process of Fe(II) ions on both NIP as well as Fe(II) IIP occurs which further decreases with an increase in the temperature indicating the exothermic nature of adsorption of Fe(II) ions [34].

3.7. Adsorption kinetic studies

Pseudo-first-order, pseudo-second-order and intraparticle diffusion models of kinetics were applied to evaluate the kinetics of the adsorption of Fe(II) ions on both NIP and Fe(II) IIP. The respective straight line equations of these kinetic models are given as follows:

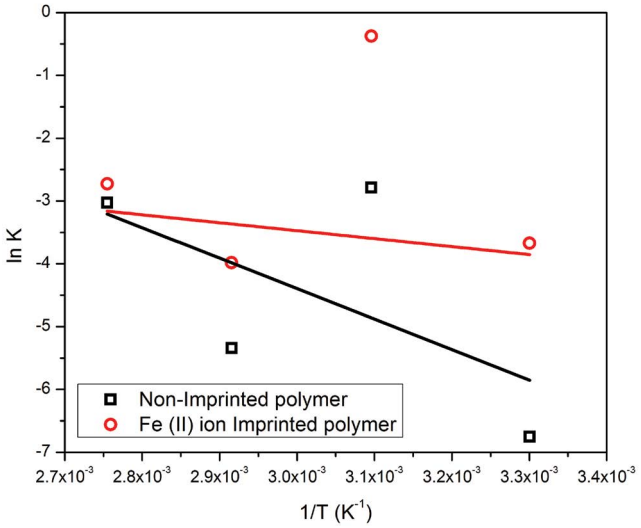

Fig. 13. Logarithmic linear plot of ln$K$ vs. 1/T for the evaluation of the thermodynamic parameters of adsorption of Fe(II) ions on non-imprinted polymer (NIP) and Fe(II) ion-imprinted polymer (IIP) adsorbent.

Table 4
Thermodynamic parameters of ΔG, ΔS, and ΔH

Adsorbent	ΔH (kJ mol^{-1})	ΔS (kJ mol^{-1})	T (K)	ΔG (kJ mol^{-1})
NIP	–40.35	0.085	298	–15.17
			323	–13.05
			343	–11.35
			363	–9.65
IIP	–10.55	0.003	298	–9.79
			323	–9.72
			343	–9.67
			363	–9.62

Pseudo-first-order kinetic model [78]

$$\ln\left(q_e - q_t\right) = \ln q_e - k_1 t \tag{27}$$

Pseudo-second-order kinetic model is [79]

$$\frac{t}{q_t} = \frac{1}{k_2 q_e^2} + \frac{t}{q_e} \tag{28}$$

where q_e shows the adsorbed amount of Fe(II) ion at equilibrium, q_t shows the adsorbed amount of Fe(II) ions at time t while k_1 and k_2 are the pseudo-first-order, pseudo-second-order rate constants respectively. The slope of the pseudo-first-order model plot of $\ln(q_e - q_t)$ against t provides the k_1 value as displayed in Fig. 14a and b whereas the intercept of the plot of t/q_t vs. t provides the k_2 value as shown in Fig. 15a and b. The kinetic parameters attained after subjecting the plots of pseudo-first and pseudo-second-order kinetic model to linear regression analysis are listed in Table 5. These values indicate that the adsorption kinetics of Fe(II) ions on both NIP and Fe(II) IIP follows pseudo-second-order model since the co-relation coefficient R^2 values which range from 0.92–0.99 for NIP and 0.96–0.99 for Fe(II) IIP for pseudo-second-order suggest best fit linearity rather than for pseudo-first-order model having values in the range of 0.87–0.99 for NIP and 0.56–0.99 for Fe(II) IIP, respectively. Similarly there is less difference between the theoretical q_e and experimental q_e for both NIP and Fe(II) IIP attained for pseudo-second-order as it does take into consideration the interaction of the solvent with the adsorbate. Hence, it can be suggested that this adsorption process of Fe(II) ions is substrate and analyte dependent that refers to the chemical adsorption phenomenon [80]. In addition, the chemical nature of the adsorption of the Fe(II) ions on the surface of the adsorbent have the chemisorption as the rate limiting step [81,82]. The difference between experimental and calculated values of the adsorption capacity is also not affected by the initial adsorbate concentration besides

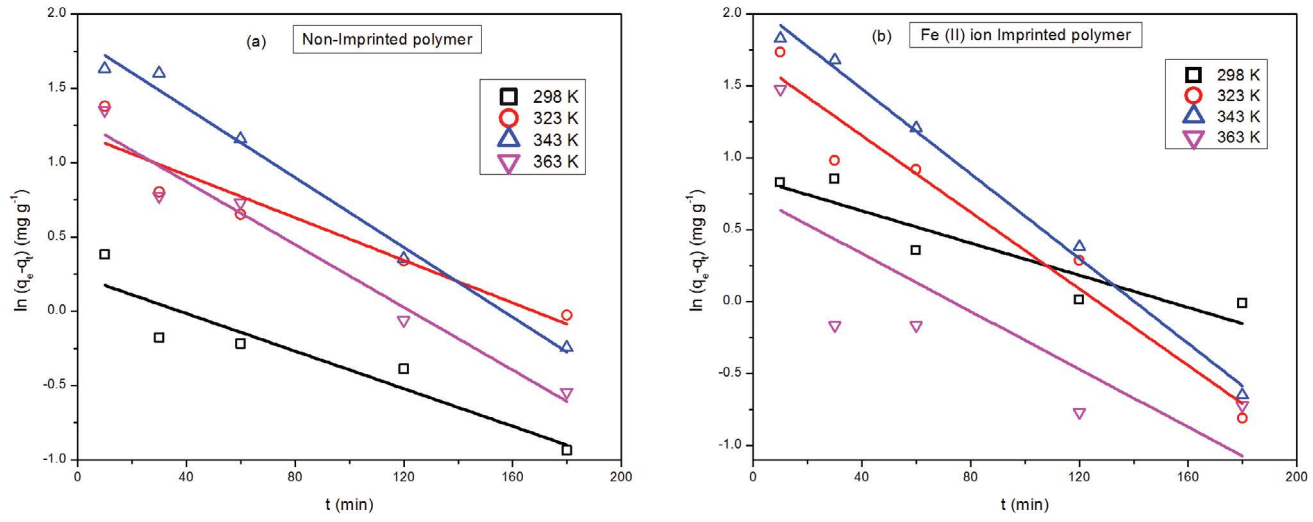

Fig. 14. Pseudo-first-order model applied on kinetic data of adsorption of Fe(II) ions on (a) non-imprinted polymer (NIP) and (b) Fe(II) ion-imprinted polymer (IIP) adsorbent at different temperatures.

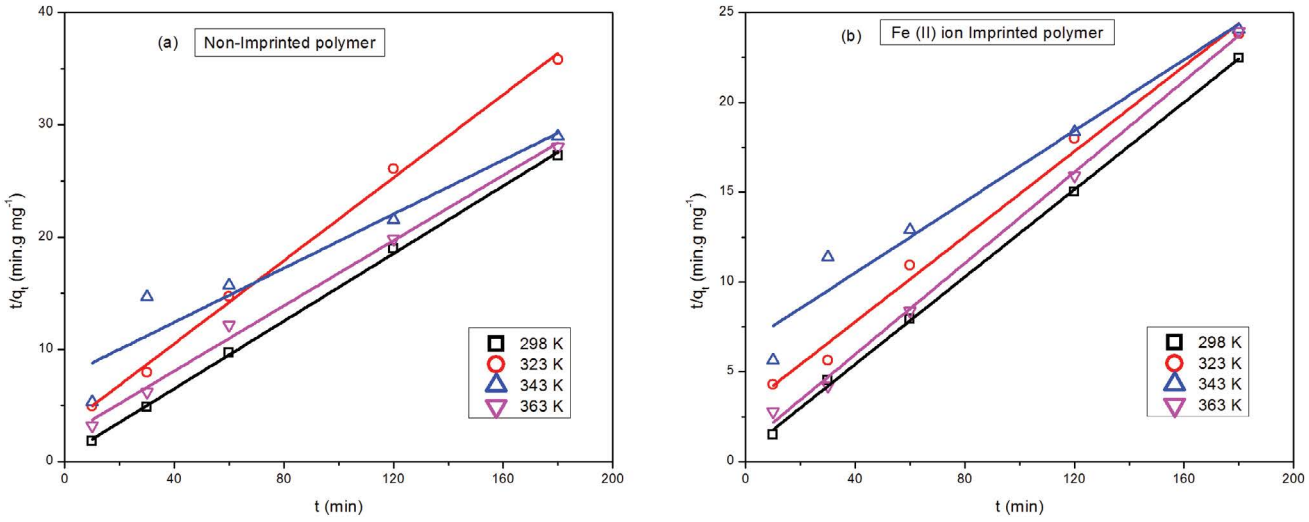

Fig. 15. Pseudo-second-order model applied on kinetic data of adsorption of Fe(II) ions on (a) non-imprinted polymer (NIP) and (b) Fe(II) ion-imprinted polymer (IIP) adsorbent at different temperatures.

the influence of the adsorbent nature [83]. Alternative explanation suggests the intrinsic simplicity of k_1 (min^{-1}) value pointing to the lack of focus on the occurrence of boundary diffusion before adsorption takes place at surface indicating a single step adsorption mechanism. Moreover, the phenomenon of adsorption in solid-liquid phase occurs in multiple steps dependent upon either dimension of pore, diffusion at surface, thin film formation of adsorbate or adsorption occurrence at heterogeneous pores sites whichever perhaps is the slow limiting step or the process is composed of multiple steps [84,85].

The adsorption kinetics rate can also be attained from the intraparticle diffusion model which regards the adsorbate diffusion towards the adsorbent surface as rate controlling step and its straight line equation is given as [86];

$$q_t = k_i t^{1/2} + C \tag{29}$$

where the adsorbed equilibrium concentration of Fe(II) is denoted as q_t and k_i represents the rate constant attained for the kinetic model of intraparticle diffusion which can be attained from the plot of $t^{1/2}$ vs q_t. Primarily, this model is based on fact that the liquid film which is established and spreads in mobile phase affects the initial beginning phase of the adsorption process only due to which it can be significantly applied to the porous adsorbents. As shown in Fig. 16a and b, three main segments of the plot of $t^{1/2}$ and q_t are evident, that is, (i) the sharp-sloped part corresponds to bulk diffusion have high adsorption rate, (ii) the linear part that follows can be attributed to the intraparticle diffusion, (iii) and the plateau segment points to the equilibrium. Similarly, the C value is attained from the intercept of the plot of $t^{1/2}$ vs. q_t that illustrates the thickness of the boundary layer [87]. The significance of this model in adsorption phenomenon is based on fact that if on obtaining straight line which passes through origin by plotting $t^{1/2}$ vs. q_t can also used to depict the rate limiting step. The intraparticle diffusion model parameters which are attained after applying linear regression are listed in Table 5, points to the fact that the linear fitting of the adsorption kinetic data was performed well suggesting that this model is obeyed at different temperature. As it is evident from the plot which did not pass through the origin that it cannot be regarded as the slow step known as rate determining step [88].

3.8. Adsorption activation energy

For determining the energy of activation of adsorption of Fe(II) ions on both NIP and Fe(II) IIP, the Arrhenius equation was applied which employ the rate constant k_2 that was taken from pseudo-second-order kinetic equation as this model of kinetics was followed by adsorption kinetics data. The activation energy E_a is obtained from the slope of the plot of lnK vs. $1/T$ as displayed in Fig. 17 according to the Arrhenius equation given in linear logarithmic form below as;

$$\ln k = \ln A - \frac{E_a}{RT} \tag{30}$$

where A is denoted as Arrhenius constant (g mg^{-1} min^{-1}), activation energy is represented as E_a (kJ mol^{-1}), universal gas constant is R (8.314 J $mole^{-1}$) and T is the absolute temperature (K). The activation energy E_a is an important parameter to differentiate the physical adsorption form the chemical adsorption, since the former have low activation energy value due to its reversible nature. On the contrary, the chemical bonds are strong and irreversible in nature due to which the activation energy value is large for chemical adsorption. The recommended range for activation energy E_a of physical adsorption is 5–40 kJ mol^{-1} as compared to 40–800 kJ mol^{-1} for chemical adsorption, respectively. According to the data listed in Table 6, it is apparent that the E_a values for both NIP and Fe(II) IIP are

Table 5
Comparison of kinetic models pseudo-first-order, pseudo-second-order and intraparticle diffusion model for adsorption of Fe(II) ions on (a) non-imprinted polymer (NIP) and (b) Fe(II) ion-imprinted polymer (IIP) adsorbent at different temperatures

Adsorption kinetic model for adsorption of						
		T (K)	$q_{e,exp}$ (mg g^{-1})	$q_{e,cal}$ (mg g^{-1})	k_1 (min^{-1})	R^2
Pseudo-first-order kinetic model	NIP	298	6.01	1.27	–0.006	0.87
		323	5.03	3.33	–0.007	0.90
		343	6.22	6.28	–0.01	0.99
		363	6.43	3.64	–0.01	0.96
	IIP	298	8.01	2.35	–0.001	0.85
		323	7.56	5.40	–0.013	0.95
		343	7.48	7.90	–0.014	0.99
		363	7.51	2.09	–0.01	0.56
		T (K)	$q_{e,exp}$ (mg g^{-1})	$q_{e,cal}$ (mg g^{-1})	k_2 (g mg^{-1} min^{-1})	R^2
Pseudo-second-order kinetic model	NIP	303	6.01	6.67	0.05	0.99
		323	5.03	5.49	0.01	0.99
		343	6.22	8.33	0.001	0.92
		363	6.43	6.89	0.009	0.99
	IIP	303	8.01	8.26	0.03	0.99
		323	7.56	8.47	0.005	0.99
		343	7.48	10.20	0.001	0.96
		363	7.51	7.94	0.02	0.99
		T (K)	$q_{e,exp}$ (mg g^{-1})	$q_{e,cal}$ (mg g^{-1})	k_i (mg g^{-1} min^{-1})	C (mg g^{-1})	R^2
Intraparticle diffusion model	NIP	303	6.01	17.23	0.09	5.79	0.83
		323	5.03	16.21	0.26	1.71	0.85
		343	6.22	18.98	0.47	0.07	0.96
		363	6.43	17.28	0.29	2.65	0.91
	IIP	303	8.01	29.76	0.15	6.17	0.87
		323	7.56	26.78	0.45	1.81	0.87
		343	7.48	10.56	0.58	–0.18	0.98
		363	7.51	7.99	0.30	4.11	0.59

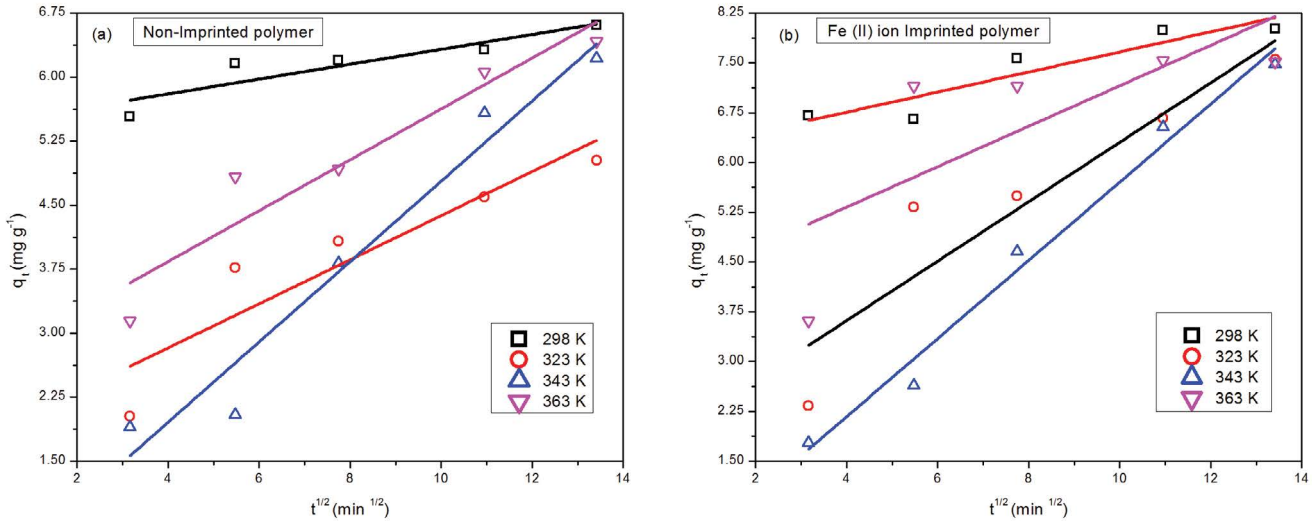

Fig. 16. Intraparticle diffusion model applied on kinetic data of adsorption of Fe(II) ions on (a) non-imprinted polymer (NIP) and (b) Fe(II) ion-imprinted polymer (IIP) adsorbent at different temperatures.

13.01 and 30.13 kJ mol^{-1}, respectively which depicts the physical nature of interaction between the Fe(II) ions and adsorbents [89].

3.9. Selectivity study

In order to perform the competitive adsorption, Fe(II) ion is mixed with different metal ions in order to attain metal ion pairs with Fe(II) ions such as Fe(II)/Co(II), Fe(II)/Cu(II), Fe(II)/Ni(II) and Fe(II)/Pb(II) which are adsorbed on NIP and Fe(II) IIP adsorbents. The similarity in charge and ionic radius of the Fe(II) ion with the interfering metal ions exist, respectively [33]. For Fe(II) IIP, the $K_{d\,(IIP)}$ values which are listed in Table 7 are high for Fe(II) ions as compared to other interfering metals such as Co(II), Cu(II), Ni(II), and Pb(II). As the surface active sites at the Fe(II) IIP formed after template removal by leaching, were complementary in size, charge, geometry and symmetry for coordination with the template imprinted ion only which result in values of k in comparison to NIP with low k value attributed to the irregular arrangement ligand functional moieties in the cross-linked polymeric matrix [90]. It is quite obvious that Fe(II) ions are adsorbed to greater limit on Fe(II) IIP adsorbent due to higher selectivity particularly for Fe(II) ion.

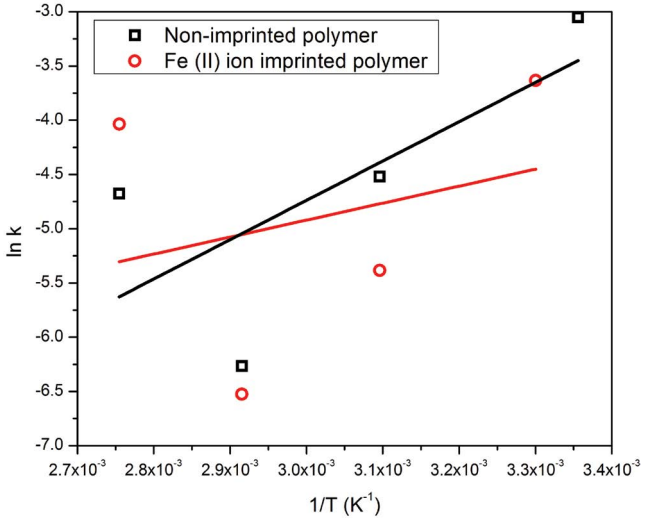

Fig. 17. Activation energy plot for adsorption of Fe(II) ions on non-imprinted polymer (NIP) and Fe(II) ion-imprinted polymer (IIP) adsorbent.

3.10. Desorption

It is obvious from Fig. 6 that with the decrease in the value of pH will render the adsorbents abundant with

Table 6
Comparison of activation energy E_a and Arrhenius constant A of Arrhenius equation applied to kinetic data of adsorption of Fe(II) ions on non-imprinted polymer (NIP) and Fe(II) ion-imprinted polymer (IIP) adsorbent

Adsorbents	A (g mg^{-1} min^{-1})	E_a (kJ mol^{-1})	R^2
NIP	6.6×10^{-05}	13.01	–0.38
IIP	1.6×10^{-07}	30.13	0.26

Table 7
Comparison of selectivity of non-imprinted polymer (NIP) and Fe(II) ion-imprinted polymer (IIP) adsorbent for adsorption of Fe(II) ions

Metal type	Fe(II) IIP		NIP		
	K_d (mL g^{-1})	k	K_d (mL g^{-1})	k	k'
Fe(II)	43.91		28.64		
Co(II)	0.98	44.76	20.73	1.38	32.41
Cu(II)	32.66	1.35	23.89	1.20	1.13
Ni(II)	21.58	2.04	18.73	1.53	1.51
Pb(II)	26.55	1.65	21.87	1.31	1.26

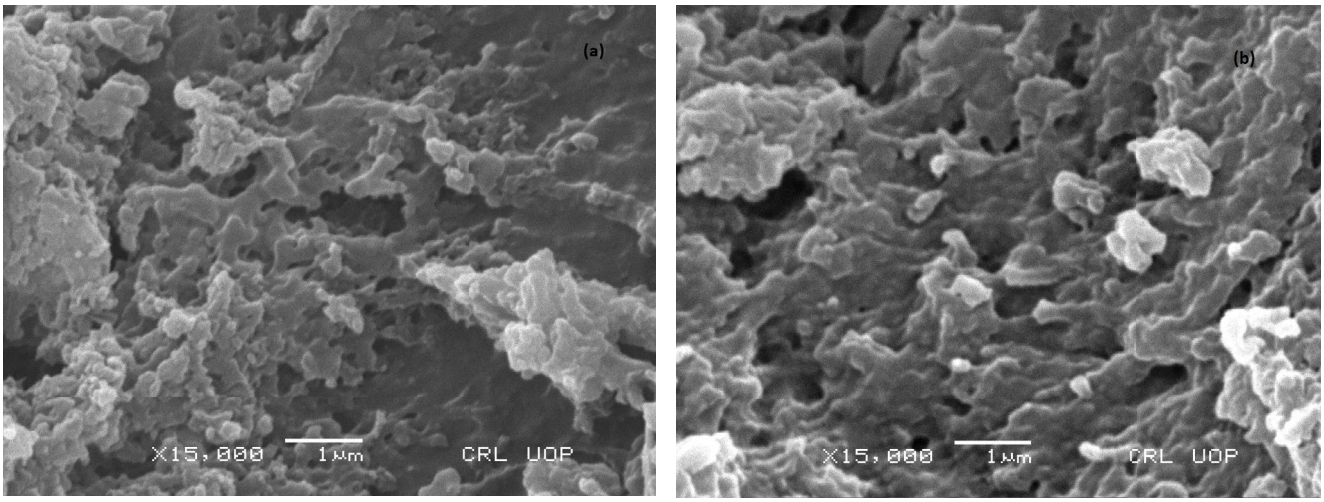

Fig. 18. SEM micrographs of (a) non-imprinted polymer (NIP) polymer and (b) Fe(II) ion-imprinted polymer (IIP) adsorbents after desorption.

Table 8
Comparison of desorption of Fe(II) ions from loaded non-imprinted polymer (NIP) and Fe(II) ion-imprinted polymer (IIP) adsorbent using 0.1 mol L^{-1} HCl aqueous solution as eluent

Fe(II) ions added (μg)	Fe(II) ions eluted (μg) (NIP)	Desorption %	Fe(II) ions eluted (μg) (IIP)	Desorption %
200	158.51	79.26	152.86	76.43
400	318.76	79.69	334.76	83.68
600	504.62	84.10	542.95	90.49

positively charged surface sites which will contribute to decrease in the Fe(II) ions interaction with the active sites. Therefore, for carrying out the elution process for regenerating the adsorbents, 0.1 N HCl aqueous solution was employed as eluting agent that will leach the metal ions from both the adsorbents. The data for the Fe(II) ion desorption is listed in Table 8. Furthermore, as depicted in Fig. 18, there is no prominent difference in the morphology of Fe(II) IIP and NIP adsorbent even after desorption indicating that surface texture and pore integrity which is suitable for adsorption is retained suggesting the physical/chemical stability to be good enough.

4. Conclusions

It is evident from the equilibrium data of the adsorption showing a prominent increase in Fe(II) IIP adsorption capacity in comparison to the NIP that corresponds to the increase in the adsorbent surface area due to the formation of surface active sites due to ion imprinting which improves the adsorption process. The electrokinetic study elaborate the pH effect on the point of zero charge (pH_{pzc}) affecting the adsorption efficiency as it is considerably greater at high pH in comparison to low pH due to adsorbent surface anionic nature at high pH. The best fit adsorption isotherm model for the equilibrium data of the adsorption was Freundlich model which corresponds to the heterogeneous nature of adsorbent surface. BET model was applied to nitrogen adsorption isotherm which revealed that the specific surface increased from 473.44 m^2 g^{-1} for NIP to 585.04 m^2 g^{-1} for Fe(II) IIP which can be attributed to the formation of surface active sites as a result of imprinting whereas on the other hand, an increment is also observed in the mesoporosity as suggested by the surface profile results attained using the *t*-plot and BJH model and it is evident as an increase in the mesopore volume from 0.369 m^2 g^{-1} for NIP to 0.418 m^2 g^{-1} for Fe(II) IIP which also enhances the adsorption efficiency, respectively. The negative values of the Gibbs free energy correspond to the spontaneity of the process which increases with temperature elevation suggesting an endothermic adsorption process. In addition, the study of the adsorption kinetics data does show that diffusion is the rate controlling step pointing to the adsorption process occurring in more than one step. Finally, the physical nature of adsorption is also confirmed by the low value of the adsorption activation energy.

Acknowledgement

This research did not receive any specific funding. The authors declare no conflicts of interest.

References

[1] K. Grefen, J. Helber, J. Heinz, F. Peters, Heavy-metals in the environment, Staub, Reinhaltung Luft, 45 (1985) 444–451.
[2] P.B. Tchounwou, C.G. Yedjou, A.K. Patlolla, D.J. Sutton, A. Luch, Heavy Metal Toxicity and the Environment, A. Luch, Ed., Molecular, Clinical and Environmental Toxicology, Vol. 3, Environmental Toxicology, Springer Science & Business Media, Berlin, 2012.
[3] S. Wang, X. Shi, Molecular mechanisms of metal toxicity and carcinogenesis, Mol. Cell. Biochem., 222 (2001) 3–9.
[4] G. Wulff, The role of binding-site interactions in the molecular imprinting of polymers, Trends Biotechnol., 11 (1993) 85–87.
[5] B.T.S. Bui, K. Haupt, Molecularly imprinted polymers: synthetic receptors in bioanalysis, Anal. Bioanal. Chem., 398 (2010) 2481–2492.
[6] K. Laatikainen, C. Branger, B. Coulomb, V. Lenoble, T. Sainio, In situ complexation versus complex isolation in synthesis of ion-imprinted polymers, React. Funct. Polym., 122 (2018) 1–8.
[7] F. Canfarotta, R. Rapini, S. Piletsky, Recent advances in electrochemical sensors based on chiral and nano-sized imprinted polymers, Curr. Opin. Electrochem., 7 (2018) 146–152.
[8] H.-T. Fan, X.-T. Sun, Z.-G. Zhang, W.-X. Li, Selective removal of lead(II) from aqueous solution by an ion-imprinted silica sorbent functionalized with chelating N-donor atoms, J. Chem. Eng. Data, 59 (2014) 2106–2114.
[9] J. Fu, L. Chen, J. Li, Z. Zhang, Current status and challenges of ion imprinting, J. Mater. Chem. A, 3 (2015) 13598–13627.
[10] F. Qiao, H. Sun, H. Yan, K.H. Row, Molecularly imprinted polymers for solid phase extraction, Chromatographia, 64 (2006) 625–634.
[11] M.J. Whitcombe, M.E. Rodriguez, P. Villar, E.N. Vulfson, A new method for the introduction of recognition site functionality into polymers prepared by molecular imprinting: synthesis and characterization of polymeric receptors for cholesterol, J. Am. Chem. Soc., 117 (1995) 7105–7111.
[12] H. Li, H. He, J. Huang, C.Z. Wang, X. Gu, Y. Gao, H. Zhang, S. Du, L. Chen, C.S. Yuan, A novel molecularly imprinted method with computational simulation for the affinity isolation and knockout of baicalein from *Scutellaria baicalensis*, Biomed. Chromatogr., 30 (2016) 117–125.
[13] H.-T. Fan, X.-T. Sun, W.-X. Li, Sol–gel derived ion-imprinted silica-supported organic–inorganic hybrid sorbent for selective removal of lead(II) from aqueous solution, J. Sol-Gel Sci. Technol., 72 (2014) 144–155.
[14] X. Chang, N. Jiang, H. Zheng, Q. He, Z. Hu, Y. Zhai, Y. Cui, Solid-phase extraction of iron(III) with an ion-imprinted functionalized silica gel sorbent prepared by a surface imprinting technique, Talanta, 71 (2007) 38–43.
[15] P.A. Cormack, A.Z. Elorza, Molecularly imprinted polymers: synthesis and characterisation, J. Chromatogr. B, 804 (2004) 173–182.
[16] K. Karim, F. Breton, R. Rouillon, E.V. Piletska, A. Guerreiro, I. Chianella, S.A. Piletsky, How to find effective functional monomers for effective molecularly imprinted polymers?, Adv. Drug Delivery Rev., 57 (2005) 1795–1808.
[17] L. Chen, S. Xu, J. Li, Recent advances in molecular imprinting technology: current status, challenges and highlighted applications, Chem. Soc. Rev., 40 (2011) 2922–2942.

[18] H.-T. Fan, W. Sun, B. Jiang, Q.-J. Wang, D.-W. Li, C.-C. Huang, K.-J. Wang, Z.-G. Zhang, W.-X. Li, Adsorption of antimony(III) from aqueous solution by mercapto-functionalized silica-supported organic–inorganic hybrid sorbent: mechanism insights, Chem. Eng. J., 286 (2016) 128–138.
[19] C. Branger, W. Meouche, A. Margaillan, Recent advances on ion-imprinted polymers, React. Funct. Polym., 73 (2013) 859–875.
[20] S. Sosnowski, M. Gadzinowski, S. Slomkowski, Poly(L,L-lactide) microspheres by ring-opening polymerization, Macromolecules, 29 (1996) 4556–4564.
[21] M. Antonietti, W. Bremser, M. Schmidt, Microgels: model polymers for the crosslinked state, Macromolecules, 23 (1990) 3796–3805.
[22] L. Ye, P.A. Cormack, K. Mosbach, Molecularly imprinted monodisperse microspheres for competitive radioassay, Anal. Commun., 36 (1999) 35–38.
[23] R. Crichton, R.R. Crichton, J.R. Boelaert, Inorganic Biochemistry of Iron Metabolism: From Molecular Mechanisms to Clinical Consequences, John Wiley & Sons, New Jersey, 2001.
[24] D.H. Boldt, New perspectives on iron: an introduction, Am. J. Med. Sci., 318 (1999) 207–212.
[25] E.R. Christensen, J.T. Delwiche, Removal of heavy metals from electroplating rinsewaters by precipitation, flocculation and ultrafiltration, Water Res., 16 (1982) 729–737.
[26] P.W. Boyd, A.J. Watson, C.S. Law, E.R. Abraham, T. Trull, R. Murdoch, D.C. Bakker, A.R. Bowie, K. Buesseler, H. Chang, A mesoscale phytoplankton bloom in the polar Southern Ocean stimulated by iron fertilization, Nature, 407 (2000) 695–702.
[27] W. Stumm, G.F. Lee, The chemistry of aqueous iron, Schweiz. Z. Hydrol., 22 (1960) 295, doi: 10.1007/BF02503278.
[28] F. An, B. Gao, X. Huang, Y. Zhang, Y. Li, Y. Xu, Z. Chen, J. Gao, Removal of Fe(II) from Ce(III) and Pr(III) rare earth solution using surface imprinted polymer, Desal. Water Treat., 51 (2013) 5566–5573.
[29] H.-T. Fan, T. Sun, Selective removal of iron from aqueous solution using ion-imprinted thiocyanato-functionalized silica gel sorbents, Korean J. Chem. Eng., 29 (2012) 798–803.
[30] H.M. Kwaambwa, A.R. Rennie, Interactions of surfactants with a water treatment protein from *Moringa oleifera* seeds in solution studied by zeta-potential and light scattering measurements, Biopolymers, 97 (2012) 209–218.
[31] A. Elaissari, Colloidal Polymers: Synthesis and Characterization, CRC Press, Florida, 2003.
[32] E. Agustina, J. Goak, S. Lee, Y. Seo, J.-Y. Park, N. Lee, Simple and precise quantification of iron catalyst content in carbon nanotubes using UV/Visible spectroscopy, ChemistryOpen, 4 (2015) 613–619.
[33] M. Mitreva, I. Dakova, I. Karadjova, Iron(II) ion-imprinted polymer for Fe(II)/Fe(III) speciation in wine, Microchem. J., 132 (2017) 238–244.
[34] T. ul Haq Zia, A.H. Mehmood, B. Ara, K. Gul, Investigation of the equilibrium, thermodynamic and kinetic parameters of study of the Allura red dye efficient removal from aqueous solution by magnetic α-Fe_2O_3 nanoparticles and its nanocomposite with graphite powder (α-Fe_2O_3/G-p), Desal. Water Treat., 139 (2019) 174–190.
[35] S.M. El-Bahy, Z.M. El-Bahy, Synthesis and characterization of polyamidoxime chelating resin for adsorption of Cu(II), Mn(II) and Ni(II) by batch and column study, J. Environ. Chem. Eng., 4 (2016) 276–286.
[36] G. Liu, X. Yang, Y. Wang, Silica/poly(*N*,*N*′-methylene-bisacrylamide) composite materials by encapsulation based on a hydrogen-bonding interaction, Polymer, 48 (2007) 4385–4392.
[37] Z. Jing, A. Xu, Y.-Q. Liang, Z. Zhang, C. Yu, P. Hong, Y. Li, Biodegradable poly(acrylic acid-co-acrylamide)/poly(vinyl alcohol) double network hydrogels with tunable mechanics and high self-healing performance, Polymers (Basel), 11 (2019) 952, doi: 10.3390/polym11060952.
[38] K.K. Bania, R.C. Deka, Experimental and theoretical evidence for encapsulation and tethering of 1,10-phenanthroline complexes of Fe, Cu, and Zn in Zeolite–Y, J. Phys. Chem. C, 116 (2012) 14295–14310.
[39] R.G. Charles, H. Freiser, R. Friedel, L.E. Hilliard, W.D. Johnston, Infra-red absorption spectra of metal chelates derived from 8-hydroxyquinoline, 2-methyl-8-hydroxyquinoline, and 4-methyl-8-hydroxyquinoline, Spectrochim. Acta, 8 (1956) 1–8.
[40] S. Brunauer, P.H. Emmett, E. Teller, Adsorption of gases in multimolecular layers, J. Am. Chem. Soc., 60 (1938) 309–319.
[41] B.C. Lippens, J.H. de Boer, Studies on pore systems in catalysts: V. The t method, J. Catal., 4 (1965) 319–323.
[42] A. Galarneau, F. Villemot, J. Rodriguez, F. Fajula, B. Coasne, Validity of the *t*-plot method to assess microporosity in hierarchical micro/mesoporous materials, Langmuir, 30 (2014) 13266–13274.
[43] E.P. Barrett, L.G. Joyner, P.P. Halenda, The determination of pore volume and area distributions in porous substances. I. Computations from nitrogen isotherms, J. Am. Chem. Soc., 73 (1951) 373–380.
[44] A.J. Bard, L.R. Faulkner, J. Leddy, C.G. Zoski, Electrochemical Methods: Fundamentals and Applications, Wiley, New York, 1980.
[45] H.-J. Butt, K. Graf, M. Kappl, Physics and Chemistry of Interfaces, John Wiley & Sons, New Jersey, 2013.
[46] M. Wiśniewska, A. Nosal-Wiercińska, I. Ostolska, D. Sternik, P. Nowicki, R. Pietrzak, A. Bazan-Wozniak, O. Goncharuk, Nanostructure of poly(acrylic acid) adsorption layer on the surface of activated carbon obtained from residue after supercritical extraction of hops, Nanoscale Res. Lett., 12 (2017) 2, doi: 10.1186/s11671-016-1772-3.
[47] M. Wiśniewska, T. Urban, E. Grządka, V.I. Zarko, V.M. Gun'ko, Comparison of adsorption affinity of polyacrylic acid for surfaces of mixed silica–alumina, Colloid Polym. Sci., 292 (2014) 699–705.
[48] M. Mackiewicz, Z. Stojek, M. Karbarz, Synthesis of cross-linked poly(acrylic acid) nanogels in an aqueous environment using precipitation polymerization: unusually high volume change, R. Soc. Open Sci., 6 (2019) 190981, doi: 10.1098/rsos.190981.
[49] T. Lee, I. Kolthoff, D. Leussing, Reaction of ferrous and ferric iron with 1,10-phenanthroline. I. Dissociation constants of ferrous and ferric phenanthroline, J. Am. Chem. Soc., 70 (1948) 2348–2352.
[50] E.F. Chaúque, L.N. Dlamini, A.A. Adelodun, C.J. Greyling, J.C. Ngila, Modification of electrospun polyacrylonitrile nanofibers with EDTA for the removal of Cd and Cr ions from water effluents, Appl. Surf. Sci., 369 (2016) 19–28.
[51] B. Ara, M. Muhammad, Rani, T.U.H. Zia, K. Gul, Selective removal of copper and cobalt from aqueous environment using new Cu(II) and Co(II) imprinted polymer and their determination by flame atomic absorption spectrophotometry, Desal. Water Treat., 191 (2020) 173–184.
[52] T. Wang, J. Wu, Y. Zhang, J. Liu, Z. Sui, H. Zhang, W.-Y. Chen, P. Norris, W.-P. Pan, Increasing the chlorine active sites in the micropores of biochar for improved mercury adsorption, Fuel, 229 (2018) 60–67.
[53] Y. Liu, Z. Liu, J. Gao, J. Dai, J. Han, Y. Wang, J. Xie, Y. Yan, Selective adsorption behavior of Pb(II) by mesoporous silica SBA-15-supported Pb(II)-imprinted polymer based on surface molecularly imprinting technique, J. Hazard. Mater., 186 (2011) 197–205.
[54] T.-H. Liou, Development of mesoporous structure and high adsorption capacity of biomass-based activated carbon by phosphoric acid and zinc chloride activation, Chem. Eng. J., 158 (2010) 129–142.
[55] S. Karaca, A. Gürses, M. Ejder, M. Açıkyıldız, Adsorptive removal of phosphate from aqueous solutions using raw and calcinated dolomite, J. Hazard. Mater., 128 (2006) 273–279.
[56] G. Belton, Langmuir adsorption, the Gibbs adsorption isotherm, and interracial kinetics in liquid metal systems, Metall. Trans. B, 7 (1976) 35–42.
[57] H. Freundlich, Über die adsorption in lösungen, Z. Phys. Chem., 57 (1907) 385–470.
[58] J. Appel, Freundlich's adsorption isotherm, Surf. Sci., 39 (1973) 237–244.
[59] F.A. Mustafai, A. Balouch, M.I. Bhanger, A. Abdullah, K. Rajar, P. Panah, B. Ahmed, T. Shah, A. Kumar, Synthesis of molecularly

imprinted polymer for the selective removal of mercury, Eur. J. Anal. Chem., 13 (2018) 5, doi: 10.29333/ejac/97222.
[60] G. Crini, P.-M. Badot, Application of chitosan, a natural aminopolysaccharide, for dye removal from aqueous solutions by adsorption processes using batch studies: a review of recent literature, Prog. Polym. Sci., 33 (2008) 399–447.
[61] M. Ismail, C.N. Weng, H.A. Rahman, N.A. Zakaria, Freundlich isotherm equilibrium equastions in determining effectiveness a low cost absorbent to heavy metal removal in wastewater (leachate) at Teluk Kitang Landfill, Pengkalan Chepa, Kelantan, Malaysia, J. Geogr. Earth Sci., 1 (2013) 1–8.
[62] F. Haghseresht, G. Lu, Adsorption characteristics of phenolic compounds onto coal-reject-derived adsorbents, Energy Fuel, 12 (1998) 1100–1107.
[63] W. Zhang, Q. Li, J. Cong, B. Wei, S. Wang, Mechanism analysis of selective adsorption and specific recognition by molecularly imprinted polymers of Ginsenoside Re, Polymers, 10 (2018) 216, doi: 10.3390/polym10020216.
[64] N.D. Hutson, R.T. Yang, Theoretical basis for the Dubinin-Radushkevitch (DR) adsorption isotherm equation, Adsorption, 3 (1997) 189–195.
[65] K. Foo, B.H. Hameed, Insights into the modeling of adsorption isotherm systems, Chem. Eng. J., 156 (2010) 2–10.
[66] E.R. Monazam, L.J. Shadle, D.C. Miller, H.W. Pennline, D.J. Fauth, J.S. Hoffman, M.L. Gray, Equilibrium and kinetics analysis of carbon dioxide capture using immobilized amine on a mesoporous silica, AIChE J., 59 (2013) 923–935.
[67] A. Ebadi, J.S.S. Mohammadzadeh, A. Khudiev, What is the correct form of BET isotherm for modeling liquid phase adsorption?, Adsorption, 15 (2009) 65–73.
[68] W.J. Weber, Physicochemical Processes for Water Quality Control, Wiley Interscience, New Jersey, 1972.
[69] Ö. Saatçılar, N. Şatıroğlu, R. Say, S. Bektas, A. Denizli, Binding behavior of Fe^{3+} ions on ion-imprinted polymeric beads for analytical applications, J. Appl. Polym. Sci., 101 (2006) 3520–3528.
[70] X. Cai, J. Li, Z. Zhang, F. Yang, R. Dong, L. Chen, Novel Pb^{2+} ion-imprinted polymers based on ionic interaction via synergy of dual functional monomers for selective solid-phase extraction of Pb^{2+} in water samples, ACS Appl. Mater. Interface, 6 (2014) 305–313.
[71] G.S. Owens, G.E. Southard, K.A.V. Houten, G.M. Murray, Molecularly imprinted ion-exchange resin for Fe^{3+}, Sep. Sci. Technol., 40 (2005) 2205–2211.
[72] S.G. Ozcan, N. Satiroglu, M. Soylak, Column solid phase extraction of iron(III), copper(II), manganese(II) and lead(II) ions food and water samples on multi-walled carbon nanotubes, Food Chem. Toxicol., 48 (2010) 2401–2406.
[73] G.-j. Zhu, H.-y. Tang, P.-h. Qing, H.-l. Zhang, X.-c. Cheng, Z.-h. Cai, H.-b. Xu, Y. Zhang, A monophosphonic group-functionalized ion-imprinted polymer for a removal of Fe^{3+} from highly concentrated basic chromium sulfate solution, Korean J. Chem. Eng., 37 (2020) 911–920.
[74] I.M. Ahmed, M.S. Gasser, Adsorption study of anionic reactive dye from aqueous solution to Mg–Fe–CO_3 layered double hydroxide (LDH), Appl. Surf. Sci., 259 (2012) 650–656.
[75] A.R. Kul, N. Caliskan, Equilibrium and kinetic studies of the adsorption of Zn(II) ions onto natural and activated kaolinites, Adsorpt. Sci. Technol., 27 (2009) 85–105.
[76] F. Zhu, L. Li, J. Xing, Selective adsorption behavior of Cd(II) ion-imprinted polymers synthesized by microwave-assisted inverse emulsion polymerization: adsorption performance and mechanism, J. Hazard. Mater., 321 (2017) 103–110.
[77] A.L.P. de Araujo, M.L. Gimenes, M.A.S.D. de Barros, M.G.C. da Silva, A kinetic and equilibrium study of zinc removal by Brazilian bentonite clay, Mater. Res., 16 (2013) 128–136.
[78] X. Ao, H. Guan, Preparation of Pb(II) ion-imprinted polymers and their application in selective removal from wastewater, Adsorpt. Sci. Technol., 36 (2018) 774–787.
[79] A.E. Regazzoni, Adsorption kinetics at solid/aqueous solution interfaces: on the boundaries of the pseudo-second-order rate equation, Colloids Surf. A., 585 (2020) 124093, doi: 10.1016/j.colsurfa.2019.124093.
[80] B. Ara, M. Muhammad, M. Salman, R. Ahmad, N. Islam, Preparation of microspheric Fe(III)-ion-imprinted polymer for selective solid phase extraction, Appl. Water Sci., 8 (2018) 41, doi: 10.1007/s13201-018-0680-3.
[81] J. Long, X. Luo, X. Yin, X. Wu, An ion-imprinted polymer based on the novel functional monomer for selective removal of Ni(II) from aqueous solution, J. Environ. Chem. Eng., 4 (2016) 4776–4785.
[82] B. Ara, M. Muhammad, H. Amin, Noori, R. Begum, S. Jabeen, S. Gul, T. ul Haq Zia, H. Nasir, Synthesis of ion-imprinted polymers by copolymerization of Zn(II) and Al(III)8-hydroxy quinolone complexes with divinylbenzene and methacryclic acid, Polym. Plast. Technol., 55 (2016) 1460–1473.
[83] Y.-S. Ho, G. McKay, The kinetics of sorption of divalent metal ions onto sphagnum moss peat, Water Res., 34 (2000) 735–742.
[84] Y.-S. Ho, G. McKay, Pseudo-second-order model for sorption processes, Process Biochem., 34 (1999) 451–465.
[85] Ö. Gerçel, A. Özcan, A.S. Özcan, H.F. Gercel, Preparation of activated carbon from a renewable bio-plant of Euphorbia rigida by H_2SO_4 activation and its adsorption behavior in aqueous solutions, Appl. Surf. Sci., 253 (2007) 4843–4852.
[86] F.-C. Wu, R.-L. Tseng, R.-S. Juang, Initial behavior of intraparticle diffusion model used in the description of adsorption kinetics, Chem. Eng. J., 153 (2009) 1–8.
[87] N. Randhawa, N. Das, R. Jana, Adsorptive remediation of Cu(II) and Cd(II) contaminated water using manganese nodule leaching residue, Desal. Water Treat., 52 (2014) 4197–4211.
[88] Z. Aly, A. Graulet, N. Scales, T. Hanley, Removal of aluminium from aqueous solutions using PAN-based adsorbents: characterisation, kinetics, equilibrium and thermodynamic studies, Environ. Sci. Pollut. Res., 21 (2014) 3972–3986.
[89] M. Doğan, H. Abak, M. Alkan, Adsorption of methylene blue onto hazelnut shell: kinetics, mechanism and activation parameters, J. Hazard. Mater., 164 (2009) 172–181.
[90] L. Wang, J. Li, J. Wang, X. Guo, X. Wang, J. Choo, L. Chen, Green multi-functional monomer based ion-imprinted polymers for selective removal of copper ions from aqueous solution, J. Colloid Interface Sci., 541 (2019) 376–386.